Nondiffusive conservative schemes based on approximate Riemann solvers for Lagrangian gas dynamics

Nina Aguillon, Christophe Chalons

Nondiffusive conservative schemes based on approximate Riemann solvers for Lagrangian gas dynamics

Nina Aguillon, Christophe Chalons

October 10, 2014

Abstract

In this paper, we present a conservative finite volume scheme for the gas dynamics in Lagrangian coordinates, which is fast and nondiffusive. Fast, because it relies on an approximate Riemann solver, and hence the costly resolution of Riemann problems is avoided. Nondiffusive, because the solution is exact when the initial data is an admissible isolated shock, and discontinuities are sharply captured in general. The construction of the scheme uses two main tools: the extension to the barotropic Euler equations of the discontinuous reconstruction strategy presented in [Agu14], and the approximate Riemann solver of [CC14], which is exact on isolated admissible shocks. Numerical experiments in 1D and 2D are proposed.

Introduction

In this paper, we consider the barotropic gas dynamics equations in Lagrangian coordinates:

$$\begin{cases} \partial_t \tau - \partial_x u = 0, \\ \partial_t u + \partial_x p(\tau) = 0, \\ \tau(0,x) = \tau^0(x), \ u(0,x) = u^0(x), \end{cases} \tag{1}$$

where the pressure law p is a strictly convex and strictly decreasing function. This system is well-known to be strictly hyperbolic, with eigenvalues $\pm\sqrt{-p'(\tau)}$ and two genuinely nonlinear characteristic fields. The phase space Ω of this system is

$$\Omega = \{(\tau, u) \in \mathbb{R}^2, \tau > 0 \ \}.$$

As usual, we supplement (1) with the validity of the so-called entropy inequality

$$\partial_t \mathcal{U}(\tau, u) + \partial_x \mathcal{W}(\tau, u) \leq 0, \tag{2}$$

where $(\mathcal{U}, \mathcal{W})$ is the entropy-entropy flux pair given by

$$\mathcal{U}(\tau, u) = \frac{u^2}{2} + e(\tau), \text{ with } e(\tau) = -\int^{\tau} p(y)dy$$

$$\mathcal{W}(\tau, u) = p(\tau)u,$$

and we consider entropy weak solutions of (1)-(2), see [GR96] for example.

In order to motivate our study, let us temporarily assume that the initial data is a Riemann initial data

$$\begin{cases} \tau^0(x) = \tau_L \mathbf{1}_{x<0} + \tau_R \mathbf{1}_{x>0}, \\ u^0(x) = u_L \mathbf{1}_{x<0} + u_R \mathbf{1}_{x>0}, \end{cases} \tag{3}$$

where the left and right states (τ_L, u_L) and (τ_R, u_R) verify the Rankine–Hugoniot relations

$$u_L - u_R = -s(\tau_L - \tau_R) \quad \text{and} \quad p(\tau_L) - p(\tau_R) = s(u_L - u_R), \tag{4}$$

for a given speed of propagation s, and the triple (τ_L, u_L), (τ_R, u_R), s satisfies (2) in the weak sense, i.e.

$$-s\left(\mathcal{U}(\tau_R, u_R) - \mathcal{U}(\tau_L, u_L)\right) + \left(\mathcal{W}(\tau_R, u_R) - \mathcal{W}(\tau_L, u_L)\right) \leq 0.$$

In that case the initial condition under consideration is such that the initial discontinuity will move at velocity s to form an admissible entropy weak solution of (1)-(2), see again [GR96]. We say that we have an isolated shock wave.

On the other hand and from the numerical point of view, the Godunov method [God59] and Godunov-type methods based on exact or approximate Riemann solvers (see [Tor09] for a review) are certainly the most celebrated numerical schemes that provide good numerical approximations of (1)-(2) for general initial data. In particular, the Lax–Wendroff theorem (see [GR96]) ensures the convergence to the entropy weak solution of (1)-(2) provided that the method does converge and verifies a discrete version of (2).

When applied to the particular initial data leading to an isolated shock wave, such conservative finite volume schemes are well-known to introduce numerical diffusion, which means here intermediate values that do not correspond to values taken by the exact solution.

The basic motivation of this work is to propose a new conservative finite volume scheme which will be able to exactly capture isolated shock waves; and more generally entropy weak solutions of (1)-(2), with no numerical diffusion near shocks. By no numerical diffusion, we mean here that only one intermediate value will be present in shock profiles and importantly that this intermediate value will correspond to the average of the exact solution on a given cell for isolated shock wave. This is of course the best one can do.

To achieve this goal, let us first emphasize that the drawbacks of Godunov and Godunov-type methods are two fold.

- First, the numerical diffusion already discussed above leads to a loss of accuracy of the approximate solutions, especially around discontinuities.

- Second, the Godunov method uses the knowledge of the exact solution of (1)-(2)-(3) with any given left and right states (τ_L, u_L) and (τ_R, u_R) in the phase space Ω. This exact Riemann solver is of course exact when (3) is an isolated shock, but it can be very expensive or difficult to compute the exact solution in general. When approximate Riemann solvers are used, it can be much less expensive but the property of being exact when (3) is an isolated shock is generally lost.

To avoid these issues, we follow the following strategy. Concerning the first point, i.e. to suppress the numerical diffusion, we use a discontinuous reconstruction strategy. The basic idea is to reconstruct entropy satisfying shocks inside some cells of the mesh in order to regain accuracy. The idea of reconstructed an initial data from the constant by cell function given by the scheme is not new. For example, in the MUSCL scheme [vL97], a linear by cell reconstruction of the solution is used. It allows to built schemes with high order on smooth regions. On the contrary, the discontinuous reconstruction strategy is not built to be precise in smooth areas, but yields to schemes that are exact on isolated shocks by the mean of allowing the reconstructed solution to have more discontinuities. This strategy was introduced in [BCLL08]. In the case of scalar advection, this scheme has an interpretation in terms of downhill decentering, and is originally presented that way in [DL01]. The case of scalar conservation law has been deeply investigated in [Lag08], [LagXX], [Bou04a] and more recently in [CDMG14]. It has been extended to the capture of contact discontinuities in [DL01] and [BFBC$^+$11]. In [ADVLCL08], [LWM08], the reader can find other nondiffusive schemes based on discontinuous reconstructions. The ENO scheme with subcell resolution [Har89] is also based on a discontinuous reconstruction; this is the only other scheme we know which is also exact on isolated shocks. In [Agu14], the discontinuous reconstruction strategy has been extended to the system of gas dynamics in Eulerien coordinates. Shocks are also sharply captured, and the proposed scheme is exact on isolated shock, but the exact Riemann solver is used. We follow this generalization to systems in the present work.

Concerning the second point, i.e. to avoid the costly exact resolution of Riemann problems which is used in [Agu14], we use the approximate solver proposed in [CC14]. Up to our knowledge, this is the first (and only) entropy consistent approximate Riemann solver which is exact for isolated shock waves. This is the key property an approximate Riemann solver should have to be coupled successfully to the discontinuous reconstruction strategy. This is exactly what we propose to do in the present paper.

To conclude this introduction, let us illustrate the fact that usual approximate Riemann solvers (abbreviated ARS in the sequel) are not exact for isolated shock waves. We consider here the Suliciu relaxation procedure [Sul98] (see also [BdL09]), which is also the starting point of the solver proposed in [CC14] and used in the present paper. The idea is to approach the solutions of (1) by the solutions of a larger but simpler system, namely

$$\begin{cases} \partial_t \tau - \partial_x u = 0, \\ \partial_t u + \partial_x \pi = 0, \\ \partial_t \mathcal{T} = \frac{1}{\epsilon}(\tau - \mathcal{T}), \end{cases} \tag{5}$$

where π is related to the pressure p via the expansion

$$\pi = \pi(\mathcal{T}) = p(\mathcal{T}) + a^2(\mathcal{T} - \tau).$$

When ϵ tends to 0, we recover asymptotically the p-system (1) we are interested in, and for stability reason a must be chosen larger than the maximum speed of the wave appearing in the initial system (1), see the next section and [Bou04b], [CLL94] and [JX95] for more details. This is the so-called subcharacteristic stability condition.

System (5) is actually simpler to solve than the original p-system (1) since the Riemann problem associated to (5), namely

$$\begin{cases} \partial_t \tau - \partial_x u = 0, \\ \partial_t u + \partial_x \pi = 0, \\ \partial_t \mathcal{T} = 0, \\ (\tau, u, \mathcal{T})(t=0,x) = (\tau_L, u_L, \mathcal{T}_L)\mathbf{1}_{x<0} + (\tau_R, u_R, \mathcal{T}_R)\mathbf{1}_{x\geq 0}, \\ \mathcal{T}_L = \tau_L \quad \text{and} \quad \mathcal{T}_R = \tau_R, \end{cases} \tag{6}$$

where the initial data is taken at equilibrium, can be explicitly solved. The characteristic fields are easily shown to be linearly degenerate, and the solution of (6) contains three contact discontinuities, propagating with velocities $-a$, 0, and a. We denote by $(\tau_{L,*}, u_{L,*}, \mathcal{T}_{L,*})$ the state on the left of the stationary wave, and by $(\tau_{R,*}, u_{R,*}, \mathcal{T}_{R,*})$ the state on its right (see Figure 1). Similarly we denote by $\pi_L := \pi(\mathcal{T}_L) = p(\tau_L)$ and $\pi_R := \pi(\mathcal{T}_R) = p(\tau_R)$.

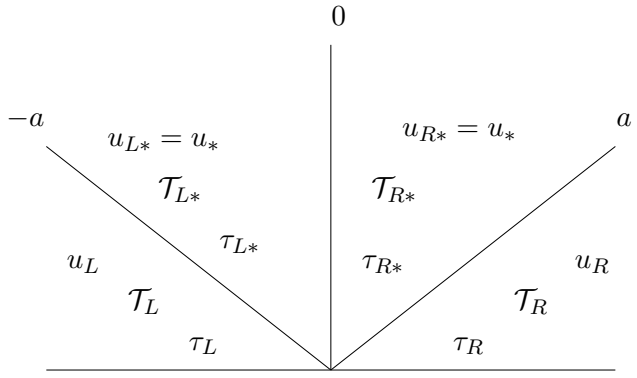

Figure 1: The approximate Riemann solver of Suliciu.

The intermediate states can be obtained using the Rankine–Hugoniot relations across each contact discontinuities, and are given by

$$\begin{cases} u_{L*} = u_{R*} := u_* = \frac{u_L + u_R}{2} - \frac{\pi_R - \pi_L}{2a}, \\ \pi_{L*} = \pi_{R*} := \pi_* = \frac{\pi_L + \pi_R}{2} - \frac{a}{2}(u_R - u_L), \\ \tau_{L*} = \tau_L + \frac{u_* - u_L}{2a}, \\ \tau_{R*} = \tau_R - \frac{u_* - u_R}{2a}, \\ \mathcal{T}_{L*} = \tau_L, \\ \mathcal{T}_{R*} = \tau_R. \end{cases} \tag{7}$$

We refer once again to [GR96] for details. Importantly, since a is chosen larger than any speed of propagation of (1) for stability reasons, there is no hope to capture exactly isolated shocks with any Godunov-type method using this approximate Riemann solver. The idea of [CC14] is to modify the approximate Riemann solver given by (6) by introducing a new

wave propagating with a velocity σ in order for the new ARS to be exact on isolated shock waves. The new wave pattern is depicted on Figure 2. Attached to this new wave is a parameter θ, which makes the link between the case of an isolated shock ($\theta = 1$, the other three waves are trivial) and the classical solver ($\theta = 0$, the new wave is trivial and the solver coincides with (7)). Moreover, this parameter can be chosen in such a way that the new ARS is entropy satisfying and exact on isolated shocks. The parameter θ can be seen as a detection parameter for shocks. Thus the shock detection step needed in [Agu14] is already enclosed in the ARS of [CC14].

This paper is organized as follows. The derivation of the scheme is detailed in the first section. More precisely, we describe the approximate solver introduced in [CC14] and the discontinuous reconstruction strategy. Then we put together the two tools and present the numerical fluxes. We prove in Subsection 1.3 that the scheme is exact whenever the initial data is an isolated shock. In the Section 2 we present 1-dimensional simulations showing that the scheme has a very low numerical dissipation. In the third and last section, we extend the scheme to 2-dimensional situation by the mean of a directional splitting. Once again, discontinuities are sharply captured.

1 Construction of the scheme

1.1 The approximate Riemann solver

In this section we briefly describe the approximate Riemann solver introduced in [CC14] to solve (1)-(2)-(3) and refer to this paper for details. The proposed approximate solution is the exact solution of the following system with Riemann initial data at equilibrium:

$$\begin{cases} \partial_t \tau - \partial_x u = 0, \\ \partial_t u + \partial_x \pi(\mathcal{T}) = 0, \\ \partial_t \mathcal{T} = \mathcal{M}(\theta)\delta_{x=\sigma t}, \\ (\tau, u, \mathcal{T})(t=0,x) = (\tau_L, u_L, \mathcal{T}_L)\mathbf{1}_{x<0} + (\tau_R, u_R, \mathcal{T}_R)\mathbf{1}_{x>0}, \\ \mathcal{T}_L = \tau_L \quad \text{and} \quad \mathcal{T}_R = \tau_R. \end{cases} \tag{8}$$

System (8) is a modified version of (5), where the measure valued right hand side $\mathcal{M}(\theta)\delta_{x=\sigma t}$ allows the solution to jump along the line $x = \sigma t$. The parameter σ is chosen such that if the initial datum is an isolated shock, σ is the exact speed of this shock. The Rankine–Hugoniot relations (4) yield

$$s^2 = -\frac{p_L - p_R}{\tau_L - \tau_R}.$$

In [CC14] the authors then propose to set

$$\sigma = \text{sign}(\tau_R - \tau_L)\sqrt{-\frac{p_L - p_R}{\tau_L - \tau_R}}, \tag{9}$$

the role of the sign function is to distinguish in between entropy shocks of the first (resp. the second) eigenvalue $-\sqrt{-p'}$ (resp. $\sqrt{-p'}$), for which the shock has a negative velocity

and $\tau_R < \tau_L$ (resp. a positive velocity and $\tau_R > \tau_L$). The parameter θ will be chosen so that the approximate Riemann solver is entropy satisfying. The solution of System (8) has four waves: the three usual waves having speeds $-a$, 0 and a, plus a wave at speed σ driven by the source term. According to [CC14], this σ-wave has to be understood as an approximation of the shock wave with the largest amplitude in the exact Riemann solution of (1)-(2)-(3). This approximation turns out to be exact in the case of an isolated shock wave. The structure of the new ARS is depicted on Figure 2.

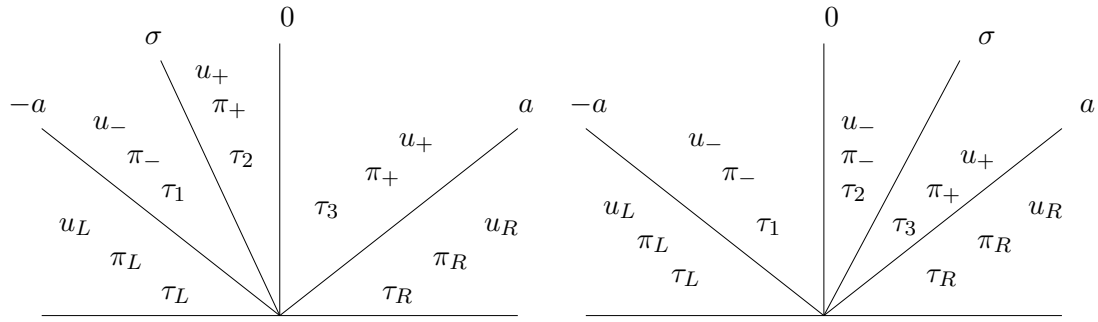

Figure 2: Structure of the Riemann solution depending on the sign of σ.

To define the three intermediate states (and hence the nine unknowns), consistency relations and Rankine–Hugoniot relations are imposed by the authors in [CC14]. We note in particular that u and τ are constant through the stationary wave while the quantity denoted by

$$\mathcal{I} = \pi(\mathcal{T}) + a^2\tau = p(\mathcal{T}) + a^2\mathcal{T} \tag{10}$$

is constant through the $-a$- and a-waves. We denote with a minus subscript (resp. a plus subscript) their values on the left (resp. on the right) of the σ-wave. The intermediate states are found by solving a *linear* system (in τ, u and $\mathcal{I}$) and are given , when $\sigma > 0$, by

$$\begin{cases} u_- &= u_* + \frac{\sigma\theta}{2a}(a-\sigma)(\tau_R-\tau_L), \\ u_+ &= u_* - \frac{\sigma\theta}{2a}(a+\sigma)(\tau_R-\tau_L), \\ \tau_1 &= \tau_L + \frac{1}{a}(u_- - u_L), \\ \tau_3 &= \tau_R + \frac{1}{a}(u_R - u_+), \\ \tau_2 &= \tau_3 - \theta(\tau_R-\tau_L), \end{cases} \quad \text{and} \quad \begin{cases} \pi_- &= \pi_* - \frac{\sigma\theta}{2}(a-\sigma)(\tau_R-\tau_L), \\ \pi_+ &= \pi_* - \frac{\sigma\theta}{2}(a+\sigma)(\tau_R-\tau_L), \\ \mathcal{I}_1 &= \mathcal{I}_L, \\ \mathcal{I}_2 &= (1-\theta)\mathcal{I}_R + \theta\mathcal{I}_L, \\ \mathcal{I}_3 &= \mathcal{I}_R. \end{cases} \tag{11}$$

and when $\sigma < 0$, by

$$\begin{cases} u_- &= u_* + \frac{\sigma\theta}{2a}(a-\sigma)(\tau_R-\tau_L), \\ u_+ &= u_* - \frac{\sigma\theta}{2a}(a+\sigma)(\tau_R-\tau_L), \\ \tau_1 &= \tau_L + \frac{1}{a}(u_- - u_L), \\ \tau_3 &= \tau_R + \frac{1}{a}(u_R - u_+), \\ \tau_2 &= \tau_1 + \theta(\tau_R-\tau_L), \end{cases} \quad \text{and} \quad \begin{cases} \pi_- &= \pi_* - \frac{\sigma\theta}{2}(a-\sigma)(\tau_R-\tau_L), \\ \pi_+ &= \pi_* - \frac{\sigma\theta}{2}(a+\sigma)(\tau_R-\tau_L), \\ \mathcal{I}_1 &= \mathcal{I}_L, \\ \mathcal{I}_2 &= (1-\theta)\mathcal{I}_L + \theta\mathcal{I}_R \\ \mathcal{I}_3 &= \mathcal{I}_R. \end{cases} \tag{12}$$

The states denoted with a star subscript $*$ correspond to intermediate states in the Suliciu ARS. Their expressions have been given in (7).

The key point of [CC14] is to pick θ is such a way that the solver satisfies a discrete entropy inequality and gives the exact solution when the initial data is an isolated shock propagating with speed s (in which case $\sigma = s$ thanks to the choice (9)). Under the classical subcharacteristic condition

$$|a| > \max_{\tau \in \{\tau_L, \tau_{L*}, \tau_{R*}, \tau_R\}} \sqrt{-p'(\tau)}, \tag{13}$$

it can be achieved with the choice

$$\begin{aligned} \sigma\theta(\mathcal{I}_R - \mathcal{I}_L) = \max\Big(0, \min\Big(&\sigma(\mathcal{I}_R - \mathcal{I}_L), -2a(a^2 - \sigma^2)\mathcal{A}(v_L, v_R), \\ &\frac{a^2|\sigma|(a+|\sigma|)}{a+|\sigma|/2}(\tau_{R*} - \tau_{L*})\mathrm{sign}(\sigma)\Big)\Big), \end{aligned} \tag{14}$$

where

$$\mathcal{A}(v_L, v_R) = \frac{\int^{\tau_R} p(s)\,ds + \frac{\pi_R}{2a^2} - \int^{\tau_L} p(s)\,ds - \frac{\pi_L}{2a^2}}{\mathcal{I}_R - \mathcal{I}_L} - \frac{\pi_*}{a^2}.$$

We recall below the main result of [CC14].

Theorem 1.1. *Under the subcharacteristic condition* (13)*, the approximate Riemann solver defined by* (9)*,* (11)*-*(12) *and* (14) *is conservative and entropy satisfying, preserves the phase space* Ω*, is Lipschitz continuous with respect to the initial Riemann data, and is exact on isolated shocks (which, again, means that if the initial condition is such that the exact solution is an isolated entropy shock wave, the proposed approximate solution coincides with the exact one).*

1.2 Discontinuous reconstruction schemes

This approximate Riemann solver will be coupled with the discontinuous reconstruction strategy introduced in [BCLL08] on the scalar conservation law with increasing flux, and extended in [Agu14] to the Euler equations using the exact Riemann solver. The aim of the discontinuous reconstruction strategy is to obtain nondiffusive conservative Godunov-type finite volume schemes, which moreover are exact for isolated and admissible shock waves. Let us first recall the formulation of finite volume schemes on a staggered grid. We denote by $t^0 = 0 < t^1 < t^2 < \cdots$ the time discretization and by $\Delta t^n = t^{n+1} - t^n$ the n-th time step. The real line is divided with cells that are always of length Δx but the cells will move at each time step. In the sequel we will also propose a scheme on a fixed grid, but for the sake of clarity it seemed more natural to begin with a (fixed-size) staggered grid. We denote by x_j^0 the centers of the cells at time t^0 and by $x_{j+1/2}^0 = x_j^0 + \Delta x/2$ their extremities. At the n-th iteration, a mesh velocity V_{mesh}^n is given, and the mesh moves from time to time according to the mesh velocity: $x_j^{n+1} = x_j^n + \Delta t^n\, V_{\mathrm{mesh}}^n$, and accordingly $x_{j+1/2}^{n+1} = x_j^{n+1} + \frac{\Delta x}{2}$. We denote by $U = (\tau, u)$ the vector of conservative variables and by $F = (-u, p(\tau))$ the flux. Integrating Equation (1) on the space-time slab

$$\left\{(t,x) \in \mathbb{R}_+ \times \mathbb{R} :\ t^n \le t < t^{n+1},\ x_{j-1/2}^n + V_{\mathrm{mesh}}^n t \le x < x_{j+1/2}^n + V_{\mathrm{mesh}}^n t\right\},$$

we obtain the scheme

$$U_j^{n+1} = U_j^n - \frac{\Delta t^n}{\Delta x}(\mathcal{F}_{j+1/2}^n - \mathcal{F}_{j-1/2}^n), \tag{15}$$

where $U_j^n = (\tau_j^n, u_j^n)$ is supposed to be an approximation of the mean value of the exact solution at time t^n on the j-th cell:

$$U_j^n \approx \frac{1}{\Delta x}\int_{x_{j-1/2}^n}^{x_{j+1/2}^n} U(t^n, x)\, dx,$$

and the numerical flux $\mathcal{F}_{j+1/2}^n = (\mathcal{F}_{j+1/2}^{n,\tau}, \mathcal{F}_{j+1/2}^{n,u})$ is an approximation of the exact flux along the line $x_{j+1/2}^n + V_{\text{mesh}}^n t$:

$$\mathcal{F}_{j+1/2}^n \approx \frac{1}{\Delta t^n}\int_{t^n}^{t^{n+1}} F(U(s, x_{j+1/2}^n + V_{\text{mesh}}^n s)) - V_{\text{mesh}}^n U(s, x_{j+1/2}^n + V_{\text{mesh}}^n s)\, ds.$$

The choice of a formula expressing $\mathcal{F}_{j+1/2}^n$ as a function of the mean values $(U_k^n)_{k\in\mathbb{Z}}$ defines the finite volume scheme. In the discontinuous reconstruction scheme presented below, the numerical flux $\mathcal{F}_{j+1/2}^n$ will depend on $(U_k^n)_{k\in\{j-1,j,j+1\}}$ when V_{mesh}^n is nonpositive and on $(U_k^n)_{k\in\{j,j+1,j+2\}}$ when V_{mesh}^n is nonnegative. The idea of the scheme is to reconstruct entropy satisfying shocks inside each cell of the mesh, using the neighboring cells, and let them evolve during a time Δt^n to compute the flux. The use of a staggered grid is crucial to avoid to deal with waves interactions, but as already stated, a natural version of the scheme on fixed grids will also be proposed.

Now, we first address the CFL restriction of time step and then we describe precisely the derivation of the discontinuous reconstruction scheme based on the ARS described in the previous section.

Moving mesh and CFL condition

For all integer j, we solve the Riemann problem $(\mathcal{R}_j)$ for the augmented system (8), with initial data at equilibrium

$$(\tau_L, u_L, \mathcal{T}_L) = (\tau_{j-1}^n, u_{j-1}^n, \tau_{j-1}^n) \quad \text{and} \quad (\tau_R, u_R, \mathcal{T}_R) = (\tau_{j+1}^n, u_{j+1}^n, \tau_{j+1}^n), \tag{16}$$

i.e. involving the neighboring cells $[x_{j-3/2}^n, x_{j-1/2}^n]$ and $[x_{j+1/2}^n, x_{j+3/2}^n]$.

We denote by $\pm a_j^n$ the speed of the extremal waves, such that (13) holds true, and by σ_j^n the speed of the additional wave (in accordance with the notation of Figure 2). We denote by $(u_{j,-}^n, u_{j,+}^n, \pi_{j,-}^n, \pi_{j,+}^n, \tau_{j,1}^n, \tau_{j,2}^n, \tau_{j,3}^n)$ the intermediate states appearing in the solution, defined by (11) or (12) (depending on the sign of σ_j^n), with (16) for the left and right states. Then, we fix a mesh velocity V_{mesh}^n such that

$$|V_{\text{mesh}}^n| \geq V_{\text{waves}}^n := \max_{k\in\mathbb{Z}} a_k^n. \tag{17}$$

The time step Δt is constrained by the CFL condition

$$\Delta t^n \leq \frac{\Delta x}{(|V_{\text{mesh}}^n| + V_{\text{waves}}^n)}. \tag{18}$$

Conditions (17) and (18) insures the following facts, that will be widely used in the sequel.

- A wave emitted at time t^n at point $x^n_{j+1/2}$ will not cross the interface $x = x^n_{j+1/2} + V^n_{\text{mesh}}t$ by (17). By (18), it will not cross the neighboring interfaces $x = x^n_{j-1/2}+V^n_{\text{mesh}}t$ and $x = x^n_{j+3/2} + V^n_{\text{mesh}}t$ within the time step either.
- More generally, a wave emitted somewhere in the cell $[x^n_{j-1/2}, x^n_{j+1/2}]$ at time t^n can only cross the interface $x = x^n_{j+1/2} + V^n_{\text{mesh}}t$ if $V_{\text{mesh}} < 0$ and the interface $x = x^n_{j-1/2} + V^n_{\text{mesh}}t$ if $V_{\text{mesh}} > 0$.
- If a wave emitted in the j-th cell interact with a wave emitted in the $j+1$-th cell this interaction occurs inside a cell and the waves created by this interaction stay in that cell and do not interact with the interface $x = x^n_{j+1/2} + V^n_{\text{mesh}}t$. This last point is true for scalar conservation law, because the velocity of the waves is smaller after the interaction than before. When considering systems of conservation law, this velocity can increase, so it is wise to overestimate V_{mesh} at least for the first iterations in time.

In practice we take, for some μ in $(0, 0.5)$ referred to as the *Courant number*,

$$\Delta t^n = \frac{\mu \Delta x}{V^n_{\text{waves}}},$$

and $V^n_{\text{mesh}} = (-1)^n \frac{\Delta x}{2\Delta t^n}$. Conditions (17) and (18) are fulfilled with this choice and we have $x^{n+1}_j = x^n_j + \frac{(-1)^n \Delta x}{2}$. Note that the mesh moves alternatively with positive and negative speeds and has always cells of size Δx.

Reconstruction of shocks

We denote by $U^n_{j,-} = (\tau^n_{j,-}, u^n_{j,-})$ and $U^n_{j,+} = (\tau^n_{j,+}, u^n_{j,+})$ the states around the σ^n_j-wave in the Riemann problem $(\mathcal{R}_j)$ (see Figure 2 for the link between $\tau_\pm$ and τ_1, τ_2, τ_3 in Formula (11) and (12)). The core of the discontinuous reconstruction strategy is to see the mean value U^n_j as the average of a shock between the state $U^n_{j,-}$ and the state $U^n_{j,+}$, located somewhere in the cell $[x^n_{j-1/2}, x^n_{j+1/2}]$ and propagating with velocity σ^n_j. This process and the notation are illustrated on Figure 3.

If we use the conservation of τ at time t^n on the cell $[x^n_{j-1/2}, x^n_{j+1/2}]$ to place the reconstructed shock, we obtain that it should lie at a distance $d^{n,\tau}_j$ of $x^n_{j-1/2}$ such that

$$d^{n,\tau}_j \tau^n_{j,-} + (\Delta x - d^{n,\tau}_j)\tau^n_{j,+} = \Delta x \tau^n_j,$$

which yields

$$d^{n,\tau}_j = \Delta x \frac{\tau^n_{j,+} - \tau^n_j}{\tau^n_{j,+} - \tau^n_{j,-}}. \tag{19}$$

Similarly, if we use the conservation of u, we obtain that it should lie at the distance

$$d^{n,u}_j = \Delta x \frac{u^n_{j,+} - u^n_j}{u^n_{j,+} - u^n_{j,-}} \tag{20}$$

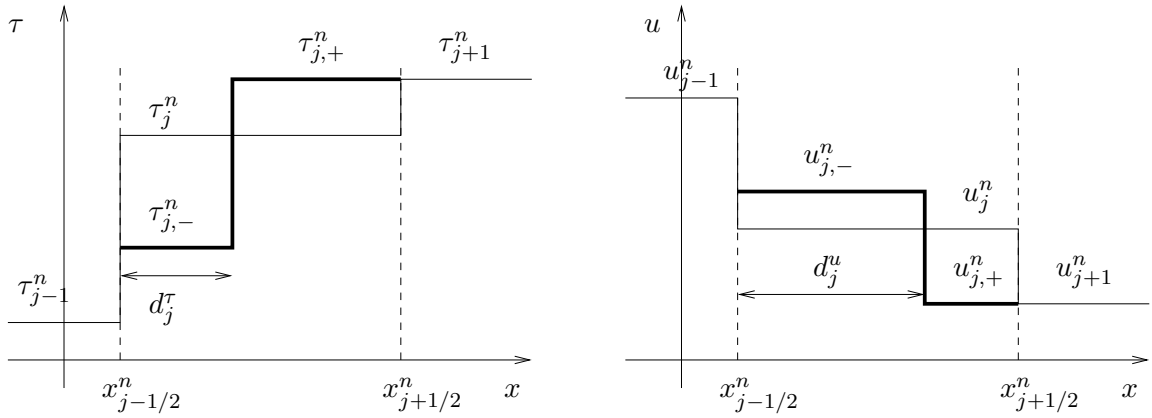

Figure 3: Toeq: Reconstruction of a shock in the j-th cell.

of $x^n_{j-1/2}$. The two distances $d^{n,\tau}_j$ and $d^{n,u}_j$ are different in general, but we will see later on that the they coincide in the case of an isolated shock wave. If one of those distances is outside of the interval $(0, \Delta x)$, we consider that the mean value in cell j does not come from the average of a shock, and we do not perform any reconstruction within the cell $[x^n_{j-1/2}, x^n_{j+1/2}]$. It yields the following definition.

Definition 1.2. The left and right reconstructed states in the j-th cell at time t^n, $(\tau^n_{j,L}, u^n_{j,L})$ and $(\tau^n_{j,R}, u^n_{j,R})$, are defined as follow:

$$(\tau^n_{j,L}, u^n_{j,L}) = \begin{cases} (\tau^n_{j,-}, u^n_{j,-}) & \text{if } d^{n,\tau}_j \in [0, \Delta x] \text{ and } d^{n,u}_j \in [0, \Delta x], \\ (\tau^n_j, u^n_j) & \text{otherwise,} \end{cases} \tag{21}$$

and

$$(\tau^n_{j,R}, u^n_{j,R}) = \begin{cases} (\tau^n_{j,+}, u^n_{j,+}) & \text{if } d^{n,\tau}_j \in [0, \Delta x] \text{ and } d^{n,u}_j \in [0, \Delta x], \\ (\tau^n_j, u^n_j) & \text{otherwise.} \end{cases} \tag{22}$$

Computation of the flux

The fluxes are computed by letting the shocks reconstructed in the previous step evolve during the time Δt^n. To illustrate the interest of using a moving mesh, consider the case illustrated in Figure 4, where a 2-shock is reconstructed in the cell $[x^n_{j-1/2}, x^n_{j+1/2}]$ and a 1-shock is reconstructed in the cell $[x^n_{j+1/2}, x^n_{j+3/2}]$ ($\sigma^n_j > 0$ and $\sigma^n_{j+1} < 0$). At time t^n, both shocks are located near $x^n_{j+1/2}$, and they will interact within the time step. As it can be seen on Figure 4, it is impossible to compute the flux on the interface $x = x^n_{j+1/2}$ (blue dotted line) without resolving the wave interaction. On the other hand, computing the flux along the interface $x = x_{j+1/2} + V^n_{\text{mesh}} t$ (red dotted line) is much easier. Under Conditions (17) and (18), this flux is piecewise constant and its computation only requires the knowledge of the crossing time between the shock reconstructed in cell j when $V^n_{\text{mesh}} < 0$ (in cell $j+1$ when $V^n_{\text{mesh}} > 0$) and the interface.

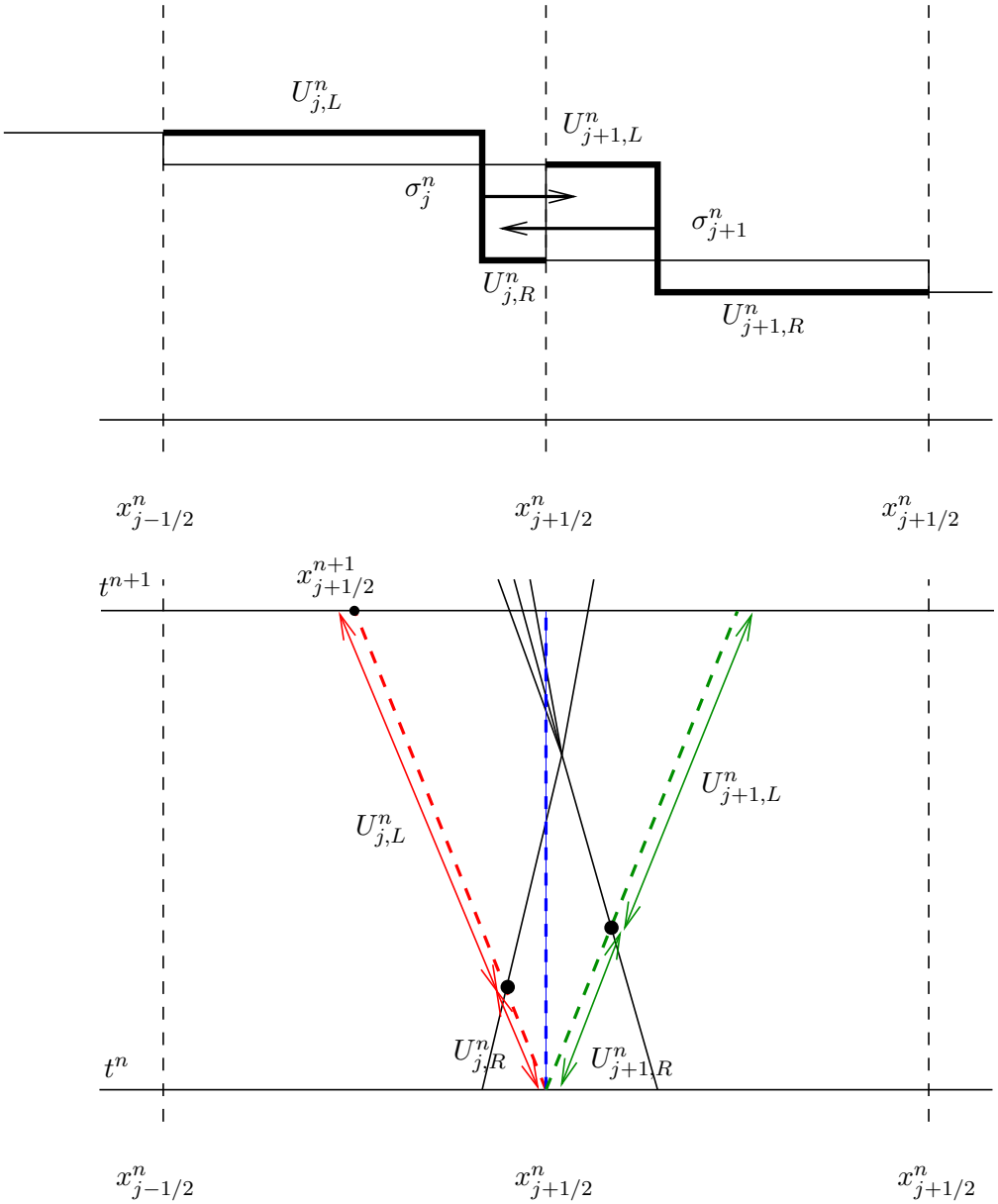

Figure 4: Top: Reconstruction of a 1-shock in the j-th cell ($\sigma^n_j > 0$) and of a 2-shock in the $j+1$-th cell ($\sigma^n_{j+1} < 0$). Bottom: in black, positions of the reconstructed shocks through times, and the waves emitted when they interact. It is easy to compute the flux through the red and green interfaces, but not through the blue one.

Let us focus on the case where V^n_{mesh} is negative. The two components of the flux are computed in the same way, except that the position of the reconstructed shock in the j-th cell at the beginning of the time step may be different for each conserved variable. More precisely, in order to compute the flux in τ, we consider that the shock reconstructed in cell $[x^n_{j-1/2}, x^n_{j+1/2}]$ is initially located at the distance $d^{n,\tau}_j$ of $x^n_{j+1/2}$. We recall that this insures the conservation of τ inside the j-th cell. As V^n_{mesh} is negative, the reconstructed shock crosses the right interface $x = x^n_{j+1/2} + V^n_{\text{mesh}} t$ at the time $T^{n,\tau}_j$ that verifies (whatever the sign of σ^n_j is)

$$d^{n,\tau}_j + \sigma^n_j T^{n,\tau}_j = \Delta x + V^n_{\text{mesh}} T^{n,\tau}_j,$$

which is

$$T^{n,\tau}_j = \frac{\Delta x - d^{n,\tau}_j}{\sigma^n_j - V^n_{\text{mesh}}}. \tag{23}$$

As we already explained, under Conditions (17) and (18), the only wave that can cross the interface $x = x^n_{j+1/2} + V^n_{\text{mesh}} t$ during the time step is the shock reconstructed in the j-th cell. Thus the flux passing through this interface (in red on Figure 4) is simply $-u_{j,R} - V^n_{\text{mesh}} \tau^n_{j,R}$ before the crossing time $T^{n,\tau}_j$ and $-u_{j,L} - V^n_{\text{mesh}} \tau^n_{j,L}$ after it. Of course, $T^{n,\tau}_j$ can be larger than Δt^n, in which case the flux is $-u_{j,R} - V^n_{\text{mesh}} \tau^n_{j,R}$ during the whole time step. Eventually the flux in τ writes

$$\begin{aligned}\Delta t \mathcal{F}^{n,\tau}_{j+1/2} = &\left(-u^n_{j,R} - V^n_{\text{mesh}} \tau^n_{j,R}\right) \min(\Delta t, T^{n,\tau}_j) \\ &+ \left(-u^n_{j,L} - V^n_{\text{mesh}} \tau^n_{j,L}\right) (\Delta t - \min(\Delta t, T^{n,\tau}_j)).\end{aligned}$$

To compute the flux in the u variable, the only difference is that the shock reconstructed in the j-th cell is initially located, using the conservation of u instead of τ, at the distance $d^{n,u}_j$ of $x^n_{j-1/2}$. Thus the crossing time is

$$T^{n,u}_j = \frac{\Delta x - d^{n,u}_j}{\sigma^n_j - V^n_{\text{mesh}}},$$

and we obtain similarly the second component of the numerical flux. Finally we have

$$\begin{cases} \Delta t \mathcal{F}^{n,\tau}_{j+1/2} = & \left(-u^n_{j,R} - V^n_{\text{mesh}} \tau^n_{j,R}\right) \min(\Delta t, T^{n,\tau}_j) \\ & + \left(-u^n_{j,L} - V^n_{\text{mesh}} \tau^n_{j,L}\right) (\Delta t - \min(\Delta t, T^{n,\tau}_j)), \\ \Delta t \mathcal{F}^{n,u}_{j+1/2} = & \left(\pi^n_{j,R} - V^n_{\text{mesh}} u^n_{j,R}\right) \min(\Delta t, T^{n,u}_j) \\ & + \left(\pi^n_{j,L} - V^n_{\text{mesh}} u^n_{j,L}\right) (\Delta t - \min(\Delta t, T^{n,u}_j)). \end{cases} \tag{24}$$

If V^n_{mesh} is positive, the only wave that can cross the interface $x = x^n_{j+1/2} + V^n_{\text{mesh}} t$ during the time step is the shock reconstructed in cell $j+1$, which propagates with velocity σ^n_{j+1}. The corresponding crossing times are

$$T^{n,\tau}_{j+1} = \frac{d^{n,\tau}_{j+1}}{V^n_{\text{mesh}} - \sigma^n_{j+1}} \quad \text{and} \quad T^{n,u}_{j+1} = \frac{d^{n,u}_{j+1}}{\sigma^n_{j+1} - V^n_{\text{mesh}}}.$$

In that case, the flux $\mathcal{F}^n_{j+1/2}$ passing through the interface is once again piecewise constant, but this time is computed with $U^n_{j+1,L}$ before the crossing time, and with $U^n_{j+1,R}$ after it (green interface on Figure 4). It writes

$$\begin{cases} \Delta t \mathcal{F}^{n,\tau}_{j+1/2} = & \left(-u^n_{j+1,L} - V^n_{\text{mesh}} \tau^n_{j+1,L}\right) \min(\Delta t, T^{n,\tau}_{j+1}) \\ & + \left(-u^n_{j+1,R} - V^n_{\text{mesh}} \tau^n_{j+1,R}\right) (\Delta t - \min(\Delta t, T^{n,\tau}_{j+1})), \\ \Delta t \mathcal{F}^{n,u}_{j+1/2} = & \left(\pi^n_{j+1,L} - V^n_{\text{mesh}} u^n_{j+1,L}\right) \min(\Delta t, T^{n,u}_{j+1}) \\ & + \left(\pi^n_{j+1,R} - V^n_{\text{mesh}} u^n_{j+1,R}\right) (\Delta t - \min(\Delta t, T^{n,u}_{j+1})). \end{cases} \tag{25}$$

Finally, the conservative variables are updated with (15).

Remark 1.3. When no reconstruction is performed, i.e. when $U^n_{j,L} = U^n_{j,R} = U^n_j$, we have, whatever the values of d^n_j, σ^n_j and T^n_j are,

$$\begin{cases} \mathcal{F}^n_{j+1/2} = F(U^n_j) & \text{if } V^n_{\text{mesh}} < 0, \\ \mathcal{F}^n_{j-1/2} = F(U^n_{j+1}) & \text{if } V^n_{\text{mesh}} > 0. \end{cases}$$

In other words in that case, the numerical fluxes (24) and (25) coincide with the staggered Lax–Friedrichs scheme, which is well-known to be stable under Conditions (17) and (18).

On a fixed grid

In this section we present a discontinuous reconstruction scheme on a fixed grid. In this section only we take $x^{n+1}_{j+1/2} = x^n_{j+1/2}$ and thus $V^n_{\text{mesh}} = 0$. There is at least three advantages in using a fixed grid:

- the Courant number can be taken in $(0, 1)$, instead of in $(0, 0.5)$ with a staggered grid. Thus we can use time step twice as large;
- at equal Courant number, the scheme on a fixed grid is less diffusive than with a staggered grid;
- dealing with boundary conditions is easier.

The problem is to deal with interactions between reconstructed shocks near an interface. The basic idea is to cancel some reconstructions when it happens. Typically in the example of Figure 4, where two reconstructed shocks cross the blue interface within the time step, we decide to cancel those two reconstructions and to use a classical numerical flux. This will be sufficient to obtain the main property of the scheme, namely to be exact when the initial data is an isolated shock.

Introducing discussion

If a shock is reconstructed in the j-th cell and has a positive speed ($\sigma^n_j > 0$), it is tempting to use the flux Formula (24) which gives the flux passing through the $j + 1/2$ interface if the initial data were

$$\begin{cases} \tau^0(x) = \tau^n_{j,L} \times \mathbf{1}_{x<x^n_{j-1/2}+d^{n,\tau}_j} + \tau^n_{j,R} \times \mathbf{1}_{x>x^n_{j-1/2}+d^{n,\tau}_j}, \\ u^0(x) = u^n_{j,L} \times \mathbf{1}_{x<x^n_{j-1/2}+d^{n,u}_j} + u^n_{j,R} \times \mathbf{1}_{x>x^n_{j-1/2}+d^{n,u}_j}, \end{cases}$$

(see what happens through the red interface of the bottom of Figure 4).

However, if a shock is reconstructed in the $j+1$ cell and has a negative speed ($\sigma_{j+1}^n < 0$), it is similarly tempting to use the flux Formula (25), which gives the flux passing through the $j+1/2$ interface if the initial data were

$$\begin{cases} \tau^0(x) = \tau_{j+1,L}^n \times \mathbf{1}_{x<x_{j+1/2}^n+d_{j+1}^{n,\tau}} + \tau_{j+1,R}^n \times \mathbf{1}_{x>x_{j+1/2}^n+d_{j+1}^{n,\tau}}, \\ u^0(x) = u_{j+1,L}^n \times \mathbf{1}_{x<x_{j+1/2}^n+d_{j+1}^{n,u}} + u_{j+1,R}^n \times \mathbf{1}_{x>x_{j+1/2}^n+d_{j+1}^{n,u}}, \end{cases}$$

(see what happens through the green interface of the bottom of Figure 4).

In the variable τ, the two shocks interact at the time $T_{j+1/2}^{n,\text{inter},\tau}$ such that

$$d_j^{n,\tau} + \sigma_j^n T_{j+1/2}^{n,\text{inter},\tau} = \Delta x + d_{j+1}^{n,\tau} + \sigma_{j+1}^n T_{j+1/2}^{n,\text{inter},\tau},$$

and we obtain a different interaction time in the variable u. We evaluate the time at which the two shocks interact by

$$T_{j+1/2}^{n,\text{inter}} = \min(T_{j+1/2}^{n,\text{inter},\tau}, T_{j+1/2}^{n,\text{inter},u}) = \min\left(\frac{d_{j+1}^n + \Delta x - d_j^n}{s_j^n - s_{j+1}^n}\right),$$

where the second minimum is taken on the two components of the vectors d_j^n and d_{j+1}^n. The interaction can also occur when when σ_j^n and σ_{j+1}^n have the same sign and $\sigma_j^n > \sigma_{j+1}^n$. If this time is smaller than Δt^n, the shocks interact within the time step and the waves created by the resulting interaction are likely to meet the $j+1/2$-th interface (which was not the case under Condition (17), see once again Figure 4). In that case, we decide to not to take into account the reconstructions in cells j and $j+1$, and to simply use the Godunov-type flux (associated with (8)) instead of the reconstruction flux (24) or (25).

Definition of the fluxes

Let us now be more precise and introduce some notation. We denote by $\mathcal{F}^{\text{GOD}}(U_L, U_R)$ the Godunov-type scheme associated to the ARS (8):

$$\mathcal{F}^{\text{GOD}}(U_L, U_R) = \begin{cases} (-u_-, \pi_-) & \text{if } \sigma > 0, \\ (-u_+, \pi_+) & \text{if } \sigma \leq 0, \end{cases} \tag{26}$$

(see Figure 2). We also denote by $\mathcal{F}_{j-1/2}^{n,\leftarrow}$ the flux given by (25) and by $\mathcal{F}_{j+1/2}^{n,\rightarrow}$ the flux given by (24). Moreover, we use the convention $\sigma_j^n = 0$ if no reconstruction is performed in cell j, and we extend the definition of the interaction time by

$$T_{j+1/2}^{n,\text{inter}} = \begin{cases} \min\left(\frac{d_{j+1}^n + \Delta x - d_j^n}{\sigma_j^n - \sigma_{j+1}^n}\right) & \text{if } \sigma_j^n > \sigma_{j+1}^n, \text{ and } \sigma_{j+1}^n \sigma_j^n \neq 0 \\ +\infty & \text{otherwise.} \end{cases} \tag{27}$$

We propose the following fluxes:

$$\mathcal{F}^n_{j+1/2} = \begin{cases} \mathcal{F}^{n,\rightarrow}_{j+1/2} & \text{if } \sigma^n_j > 0,\ T^{n,\text{inter}}_{j+1/2} > \Delta t \text{ and } \sigma^n_{j+1} \geq 0, \\ \mathcal{F}^{n,\leftarrow}_{j+1/2} & \text{if } \sigma^n_{j+1} < 0,\ T^{n,\text{inter}}_{j+1/2} > \Delta t \text{ and } \sigma^n_j \leq 0, \\ \mathcal{F}^{\text{GOD}}(U^n_j, U^n_{j+1}) & \text{if } (\sigma^n_j > 0 \text{ and } \sigma^n_{j+1} < 0) \text{ or } T^{n,\text{inter}}_{j+1/2} \leq \Delta t, \\ \mathcal{F}^{\text{GOD}}(U^n_{j,R}, U^n_{j+1,L}) & \text{otherwise.} \end{cases} \tag{28}$$

In particular for simplicity, we cancel the reconstructions in cells j and $j+1$ if $\sigma^n_j > 0$ and $\sigma^n_{j+1} < 0$. We now justify the choice of flux $F^{n,\rightarrow}_{j+1/2}$ if $\sigma^n_j > 0$ and $\sigma^n_{j+1} = 0$, which corresponds to the case where a shock with positive speed is reconstructed in the j-th cell but no shock is reconstructed in the $j+1$-th cell. In that case the $-a^n_j$, 0 and σ^n_j-waves in the solution of (8) with the left state $U^n_{j,R}$ and the right state U^n_{j+1} are trivial, and only the a^n_j-wave is nontrivial. Thus, as $a^n_j > \sigma^n_j$ and as depicted on Figure 5, no wave interaction occur at interface $j+1/2$. The flux through the interface $j+1/2$ is easily computed and given by $\mathcal{F}^{n,\rightarrow}_{j+1/2}$.

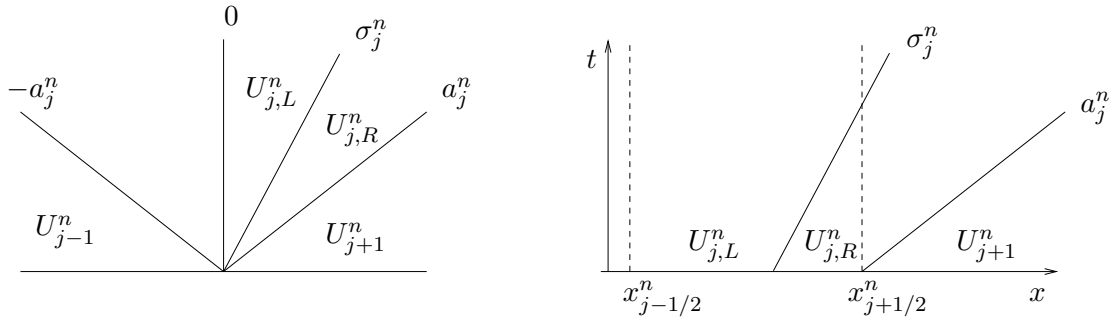

Figure 5: Left: the structure of the ARS used to determine $U^n_{j,L}$ and $U^n_{j,R}$. Right: the waves emitted in the reconstructed solution: there is only a wave at speed a^n_j between $U^n_{j,R}$ and U^n_{j+1}, which is faster than the reconstructed shock. Thus the flux through the interface $j+1/2$ is easily computed and given by $\mathcal{F}^{n,\rightarrow}_{j+1/2}$.

We now prove a nontrivial property that states that if the initial data is an isolated shock wave, the discontinuous reconstruction scheme (on a staggered or on a fixed grid) is exact.

1.3 Exact approximation of isolated shocks

Let us start this section by the following proposition, which is easily verified.

Proposition 1.4. *The numerical fluxes* (24) *and* (25) *(on a staggered grid) and* (28) *(on a fixed grid) are consistent: if* $U^n_{j-1} = U^n_j = U^n_{j+1} = U^n_{j+2} := U$, *then* $\mathcal{F}^n_{j+1/2} = f(U) - V^n_{\text{mesh}} U$ *(we recall that on a fixed grid,* $V^n_{\text{mesh}} = 0$*).*

The aim of this subsection is to prove the following theorem.

Theorem 1.5. *The discontinuous reconstruction scheme is exact whenever the initial data is an isolated entropy satisfying shock. More precisely, suppose that the initial data is*

$$\begin{cases} \tau^0(x) = \tau_L \mathbf{1}_{x<0} + \tau_R \mathbf{1}_{x>0} \\ u^0(x) = u_L \mathbf{1}_{x<0} + u_R \mathbf{1}_{x>0} \end{cases}$$

with $u_L > u_R$ and (τ_L, u_L) and (τ_R, u_R) linked by the Rankine–Hugoniot relations (4). Then U_j^n is the average of the exact solution at time t^n over the interval $[x_{j-1/2}^n, x_{j+1/2}^n]$ for all j in $\mathbb{Z}$.

Remark 1.6. In particular, this theorem means that for such particular initial data, no spurious numerical diffusion is created by the scheme. For general initial data, the same behavior is observed, see Section 2 below.

Proof. We prove the result for a 1-shock (the reasoning is similar for a 2-shock), thus in the following we suppose that $\tau_L > \tau_R$. Suppose that the property is verified for an integer n. Then, there exists an integer j_0^n and a distance $d_{j_0}^n \in [0, \Delta x]$ such that

$$U_k^n = \begin{cases} U_L & \text{if } k < j_0^n, \\ \frac{d_{j_0}^n}{\Delta x} U_L + \frac{\Delta x - d_{j_0}^n}{\Delta x} U_R & \text{if } k = j_0^n, \\ U_R & \text{if } k > j_0^n. \end{cases}$$

By construction, the approximate Riemann solver of [CC14] is exact on $(\mathcal{R}_{j_0^n})$. Therefore, the shock is correctly reconstructed in cell j_0^n, it by (9) has the correct speed

$$\sigma := \frac{u_L - u_R}{\tau_R - \tau_L}.$$

The two distances $d_{j_0^n}^\tau$ and $d_{j_0^n}^u$ given by (19) and (20) are both equal to $d_{j_0^n}^n$, and correspond to the exact position of the shock at time t^n. On the other hand, no reconstruction is performed in cells $j_0^n - 1$ and $j_0^n + 1$, because it is impossible to have $d_{j_0^n-1}^{n,\tau}$ or $d_{j_0^n+1}^{n,\tau}$ in $(0, \Delta x)$.

Let us indeed explain in detail the case of the cell $j_0^n - 1$. Consider the Riemann problem between the left state (τ_L, u_L) and $(\tilde{\tau}_R, \tilde{u}_R) := (\alpha\tau_R + (1-\alpha)\tau_L, \alpha u_R + (1-\alpha)u_L)$, where $\alpha = \frac{d_{j_0^n}^n}{\Delta x}$. We denote by $\tilde{\sigma}$ the speed of the shock wave in this Riemann problem, which by (9) is given by

$$\tilde{\sigma} := \sqrt{\frac{p_L - \tilde{p}_R}{\tilde{\tau}_R - \tau_L}}, \quad \text{where} \quad \tilde{p}_R = p(\tilde{\tau}_R).$$

As $\tau_+ \geq \tau_-$, if τ_- is larger than τ_L, it is impossible to reconstruct τ in cell $j_0^n - 1$ in a

conservative manner. The difference $\tau_- - \tau_L$ expresses as a function of θ:

$$\begin{aligned}\tau_-(\theta) - \tau_L &= \tau_+(\theta) - \theta(\tilde{\tau}_R - \tau_L) - \tau_L \\ &= \tilde{\tau}_R + \frac{1}{a}(\tilde{u}_R - u_+(\theta)) - \theta(\tilde{\tau}_R - \tau_L) - \tau_L \\ &= (1-\theta)(\tilde{\tau}_R - \tau_L) + \frac{1}{a}\left(\tilde{u}_R - u_* + \frac{\tilde{\sigma}\theta}{2a}(a+\tilde{\sigma})(\tilde{\tau}_R - \tau_L)\right) \\ &= (\tilde{\tau}_R - \tau_L) + \frac{\tilde{u}_R - u_*}{a} - \theta(\tilde{\tau}_R - \tau_L)\left(1 - \frac{\tilde{\sigma}}{2a^2}(a+\tilde{\sigma})\right).\end{aligned}$$

This function is decreasing with respect to θ. Indeed, $\tilde{\tau}_R$ is larger than τ_L, and as a is larger than $\tilde{\sigma}$ we have

$$\frac{\tilde{\sigma}(a+\tilde{\sigma})}{2a^2} \leq 1.$$

Thus for all θ in $[0,1]$,

$$\begin{aligned}\tau_-(\theta) - \tau_L &= \tau_-(\theta = 1) - \tau_L \\ &= \frac{1}{a}\left(\tilde{u}_R - u_* + \frac{\tilde{\sigma}}{2a}(a+\tilde{\sigma})(\tilde{\tau}_R - \tau_L)\right).\end{aligned}$$

Let us prove that the quantity

$$Q := \tilde{u}_R - u_* + \frac{\tilde{\sigma}}{2a}(a+\tilde{\sigma})(\tilde{\tau}_R - \tau_L)$$

is positive. Replacing u_* by its value, we obtain

$$Q = \frac{\tilde{u}_R - u_L}{2} + \frac{\tilde{\pi}_R - \pi_L}{2a} + \frac{\tilde{\sigma}}{2a}(a+\tilde{\sigma})(\tilde{\tau}_R - \tau_L).$$

Now, we divide by $\tilde{\tau}_R - \tau_L$ and use the definition of $\tilde{\sigma}$ to write

$$\frac{2Q}{\tilde{\tau}_R - \tau_L} = -\sigma - \frac{\tilde{\sigma}^2}{a} + \frac{\tilde{\sigma}}{a}(a+\tilde{\sigma}) = \tilde{\sigma} - \sigma$$

We conclude by remarking that as the pressure is convex,

$$\tilde{\pi}_R = p(\alpha\tau_R + (1-\alpha)\tau_L) \leq \alpha\pi_R + (1-\alpha)\pi_L$$

and thus

$$\tilde{\sigma} = \sqrt{\frac{\pi_L - \tilde{\pi}_R}{\tilde{\tau}_R - \tau_L}} \geq \sqrt{\frac{\pi_L - \pi_R}{\tau_R - \tau_L}} = \sigma.$$

Proving that no reconstruction is performed in cell $j_0^n + 1$ follows the same lines. We now focus on the Riemann problem between the left state $(\tilde{\tau}_L, \tilde{u}_L) := (\alpha\tau_L + (1-\alpha)\tau_R, \alpha u_L +$

$(1-\alpha)u_R)$ and (τ_R, u_R). We have

$$\begin{aligned} u_+ - u_R &\geq u_* - \frac{\tilde{\sigma}}{2a}(a+\tilde{\sigma})(\tau_R - \tilde{\tau}_L) - u_R \\ &= \frac{\tilde{u}_L - u_R}{2} - \frac{\pi_R - \tilde{\pi}_L}{2a} - \frac{\tilde{\sigma}}{2a}(a+\tilde{\sigma})(\tau_R - \tilde{\tau}_L) \\ &= \frac{\tau_R - \tilde{\tau}_L}{2}\left(\sigma + \frac{\tilde{\sigma}^2}{a} - \frac{\tilde{\sigma}}{a}(a+\tilde{\sigma})\right) \\ &= \frac{\tau_R - \tilde{\tau}_L}{2}\left(\sigma - \tilde{\sigma}\right). \end{aligned}$$

It follows that u_+ is larger than u_R, because

$$\tilde{\sigma} = \sqrt{\frac{\tilde{\pi}_L - \pi_R}{\tau_R - \tilde{\tau}_L}} \leq \sqrt{\frac{\pi_L - \pi_R}{\tau_R - \tau_L}} = \sigma.$$

Thus, $\tau_+ = \tau_R + \frac{1}{a}(u_R - u_+)$ is smaller than τ_L, and as τ_- is smaller than τ_+, it is impossible to reconstruct τ.

The rest of the proof consists in an elementary checking that (24) and (25) give the correct flux, it can be found in [Agu14]. The case of a fixed grid follows because no reconstruction is cancelled.

□

2 One dimensional numerical simulations

2.1 Riemann problems

To begin with we test the discontinuous reconstruction scheme on a staggered grid. The space interval $[-1, 1]$ is discretized with 100 cells and the pressure law is $p(\tau) = \tau^{-2}$. We take

$$\Delta t^n = 0.45\frac{\Delta x}{V^n_{\text{waves}}} \quad \text{and} \quad V^n_{\text{mesh}} = (-1)^n \frac{\Delta x}{2\Delta t^n},$$

thus both (17) and (18) hold. In each cases, we compare the discontinuous reconstruction scheme and the Godunov-type scheme, both based on the approximate Riemann solver of [CC14]. The flux of the "Godunov-type scheme" is computed on a fixed grid ($V^n_{\text{mesh}} = 0$) and its expression is given in (26).

The first three test cases are taken from [CC14], the fourth one is a variant of the fast shock of Arora and Roe [AR97]. On those test cases, the results given by the proposed schemes on staggered and fixed grids are very close to each other (the scheme on a fixed grid being less diffusive in general, but with almost no impact here). This is why we only show the results given by the scheme on a staggered grid.

Test 1: Isolated shock

The first Riemann problem is

$$\tau_L = 1,\ u_L = 0,\ \tau_R = 0 \quad \text{and} \quad u_R = -\sqrt{3}/2.$$

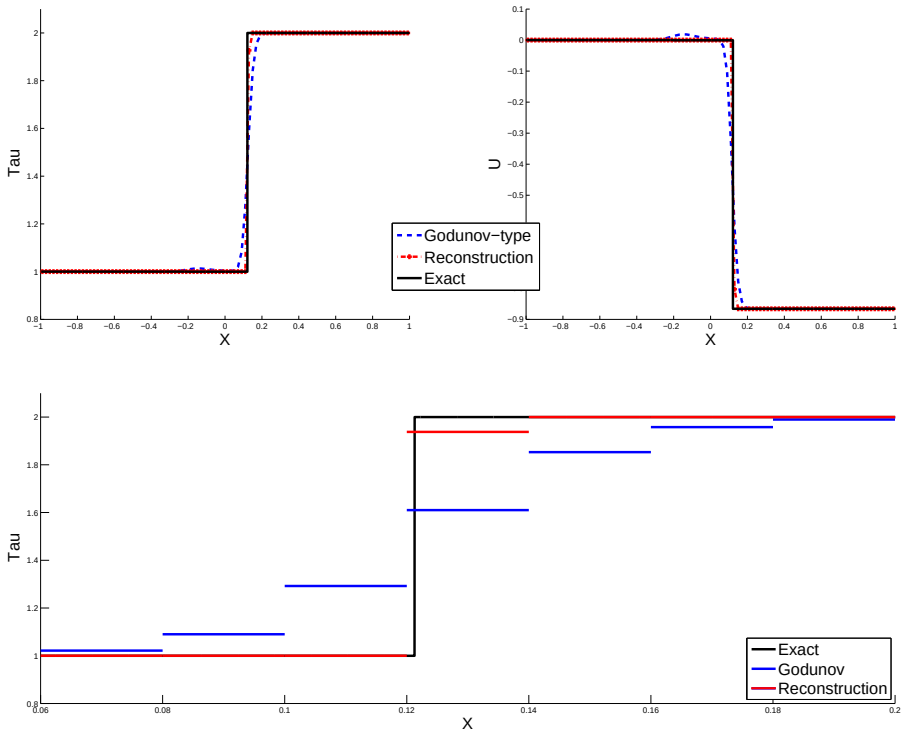

Figure 6: Test 1 : specific volume (top left) and velocity (top right) at time $t = 0.15$. Bottom: close-up on the piecewise constant shock profile.

It corresponds to an isolated shock. Theorem 1.5 is illustrated on Figure 6: the shock is perfectly advected by the reconstruction scheme, while it is diffused by the Godunov-type scheme. On the bottom of this figure, we can see that there is only one intermediate value in the shock profile given by the reconstruction scheme, which corresponds to the average of the exact solution on the cell.

Test 2: Rarefaction and shock

The second Riemann problem corresponds to

$$\tau_L = 0.3,\ u_L = 0,\ \tau_R = 0.6 \quad \text{and} \quad u_R = 0.$$

It contains a 1-rarefaction wave and a 2-shock. On Figure 7, we can see that the shock is sharply captured by the reconstruction scheme.

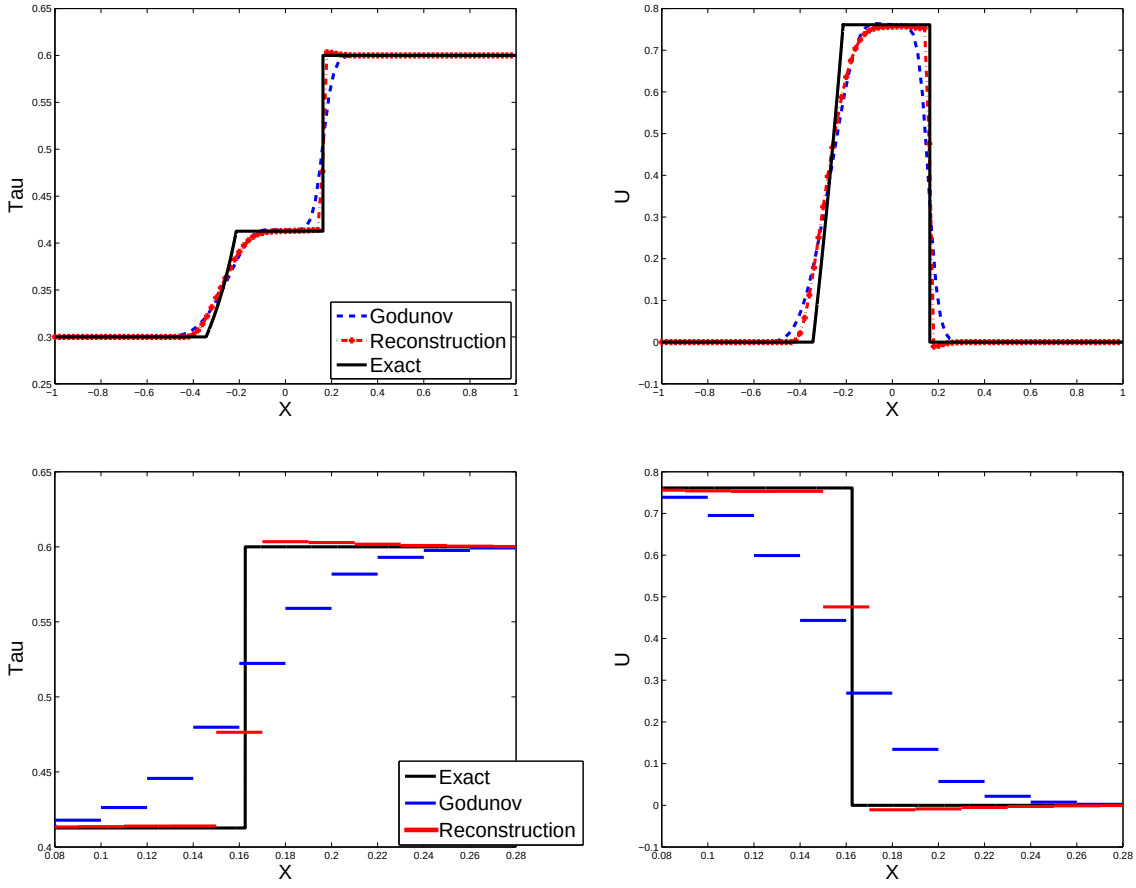

Figure 7: Test 2 : specific volume (top left) and velocity (top right) at time $t = 0.04$. Bottom: close-up on the piecewise constant shock profile.

Test 3: Shock and shock

Here the Riemann problem corresponds to

$$\tau_L = 0.5,\ u_L = 2,\ \tau_R = 0.6 \quad \text{and} \quad u_R = 1.$$

It contains a 1-shock and a 2-shock. Figure 8 clearly demonstrates that they are both sharply captured, with only one point of numerical diffusion.

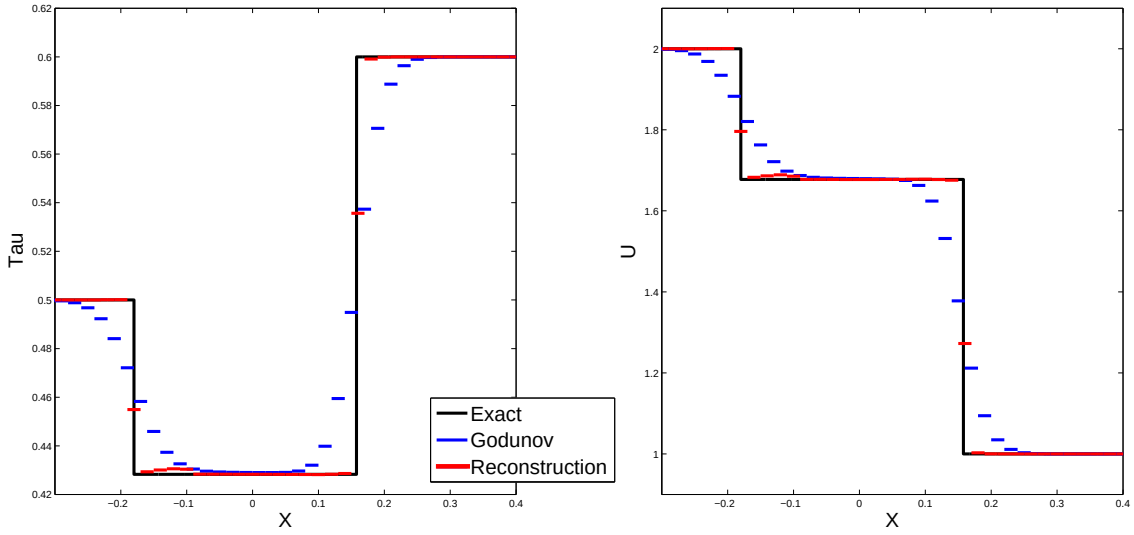

Figure 8: Test 3 : specific volume (top left) and velocity (top right) at time $t = 0.05$.

Test 4: shock and strong shock

For this test case we have

$$\tau_L = 1,\ u_L = 1,\ \tau_R = 52 \quad \text{and} \quad u_R = -8,$$

which is a slight modification of the isolated fast shock considered in [AR97]. When computing a strong shock (also called fast shock), spurious oscillations appear in the velocity when using usual Godunov-type methods. They also appear clearly in the characteristic variable $u \pm \sqrt{8/\tau}$. Those two quantities are plotted on Figure 9. Theorem 1.5 states that the scheme is exact on isolated strong shocks. We can see on Figure 9 that the ability of the reconstruction scheme to approach correctly fast shocks is not lost when we introduce a perturbation (here, a second wave in the Riemann problem).

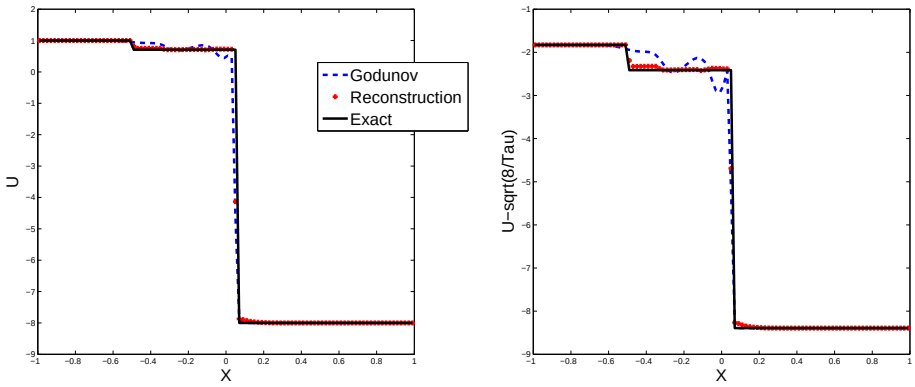

Figure 9: Test 4 : velocity (left) and $u - \sqrt{8/\tau}$ (right) at time $t = 0.3$.

Test 5: Isentropic compression

This test case consists in reversing the time starting from a developed 1-rarefaction wave, to recover a discontinuity. This is a difficult test case. More precisely, let us denote

$$(t, x) \mapsto U_{\text{rar}}(x/t; U_L, U_R) = (\tau_{\text{rar}}(x/t; U_L, U_R), u_{\text{rar}}(x/t; U_L, U_R))$$

the self-similar rarefaction wave associated with the Riemann initial condition $U_L \mathbf{1}_{x<0} + U_R \mathbf{1}_{x\geq 0}$, with $U_L = (\tau_L, u_L)$, $U_R = (\tau_R, u_R)$ and

$$\tau_L = 0.5,\ u_L = 10,\ \tau_R = 5 \quad \text{and} \quad u_R = u_L - \sqrt{2}(\tau_R^{-1/2} - \tau_L^{-1/2}).$$

For this test case, the initial data is

$$\tau^0(x) = \tau_{rar}(-x/T_{\text{rar}}) \quad u^0(x) = u_{rar}(-x/T_{\text{rar}})$$

with $T_{\text{rar}} = 0.2$. This initial condition is plotted on Figure 10.

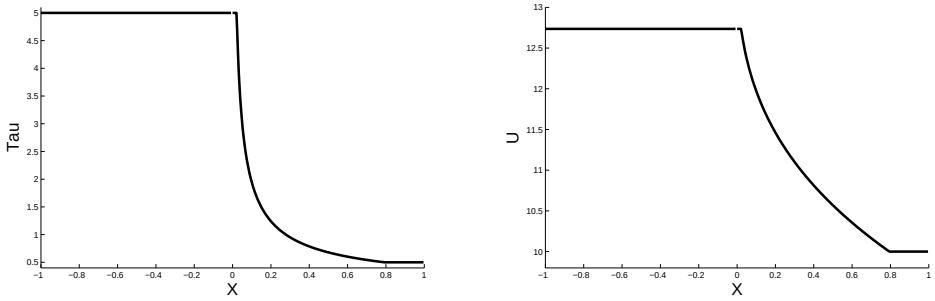

Figure 10: Initial condition for test 5.

For times $t < T_{\text{rar}}$, the exact solution is $U(t, x) = U_{rar}(-x/(T_{\text{rar}} - t))$, and for times $t \geq T_{\text{rar}}$, the solution coincides with the solution of the Riemann problem associated with

left state U_R and *right* state U_L (at time $t - T_{\text{rar}}$), which contains a 1-shock and a 2-rarefaction. In particular at time $t = T_{\text{rar}}$ the exact solution is nothing but a discontinuity between U_R and U_L and located at $x = 0$.

We compare the reconstruction scheme on a staggered grid (abbreviated `RecSG` in the legends) and on a fixed grid (abbreviated `RecFG`) at five different times. This is the only test case where the results are significantly different for the two schemes. On Figures 11 and 12 we plot the solutions for $t = 0.14$, $t = 0.17$, $t = 0.2$, $t = 0.23$ and $t = 0.26$. We observe a spike near the discontinuity when the time t is close to T_{rar}. It seems that the reconstruction scheme starts to reconstruct a little before $t = T_{\text{rar}}$ the expected shock that will appear in the exact solution for times $t > T_{\text{rar}}$, and that will be eventually sharply computed by the proposed scheme. The maximal height of the spike is at $t = T_{\text{rar}}$, and it diminishes rapidly afterwards, the shock being correctly approximated after T_{rar}. The spike does not prevent the scheme from converging in L^1, and its size is independent from the Courant number. On this test case, we observe that on the left of the solution, the results given on a fixed grid are much better than the ones given on a staggered grid. On the other hand, we note that the Godunov-type scheme does not create any spike, but introduces numerical diffusion on the shock wave for times $t > T_{\text{rar}}$, as it is expected.

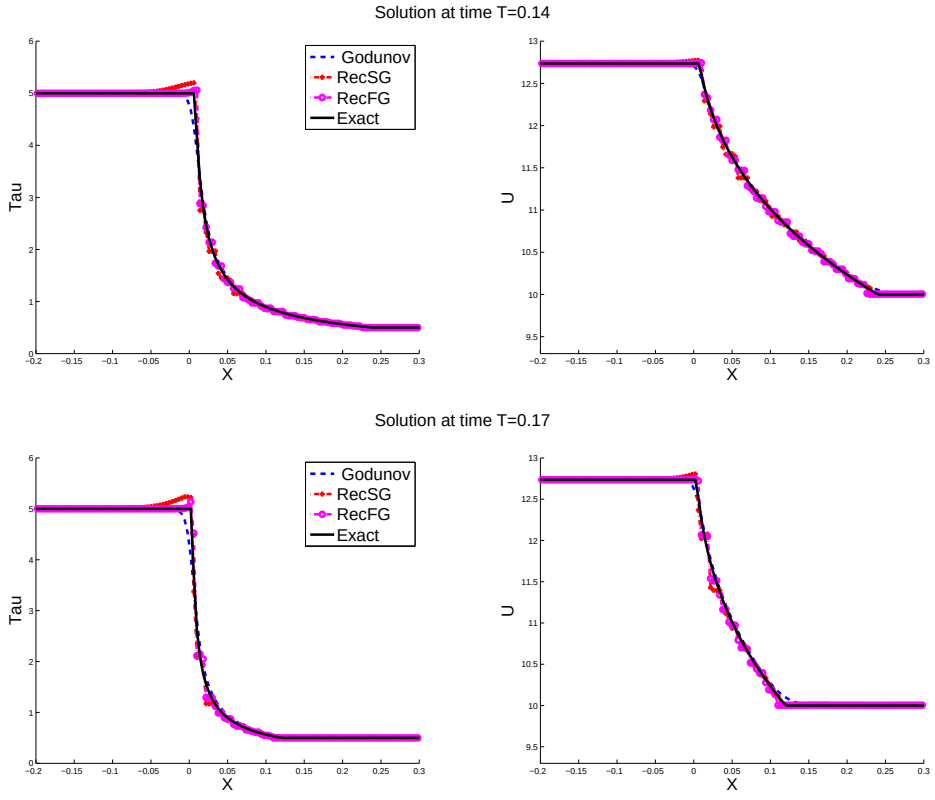

Figure 11: Solution of test 5 with, from top to bottom, $t = 0.14$ and $t = 0.17$.

On Figure 13, we plot the evolution of the entropy during the time interval $[0, 4]$ for this

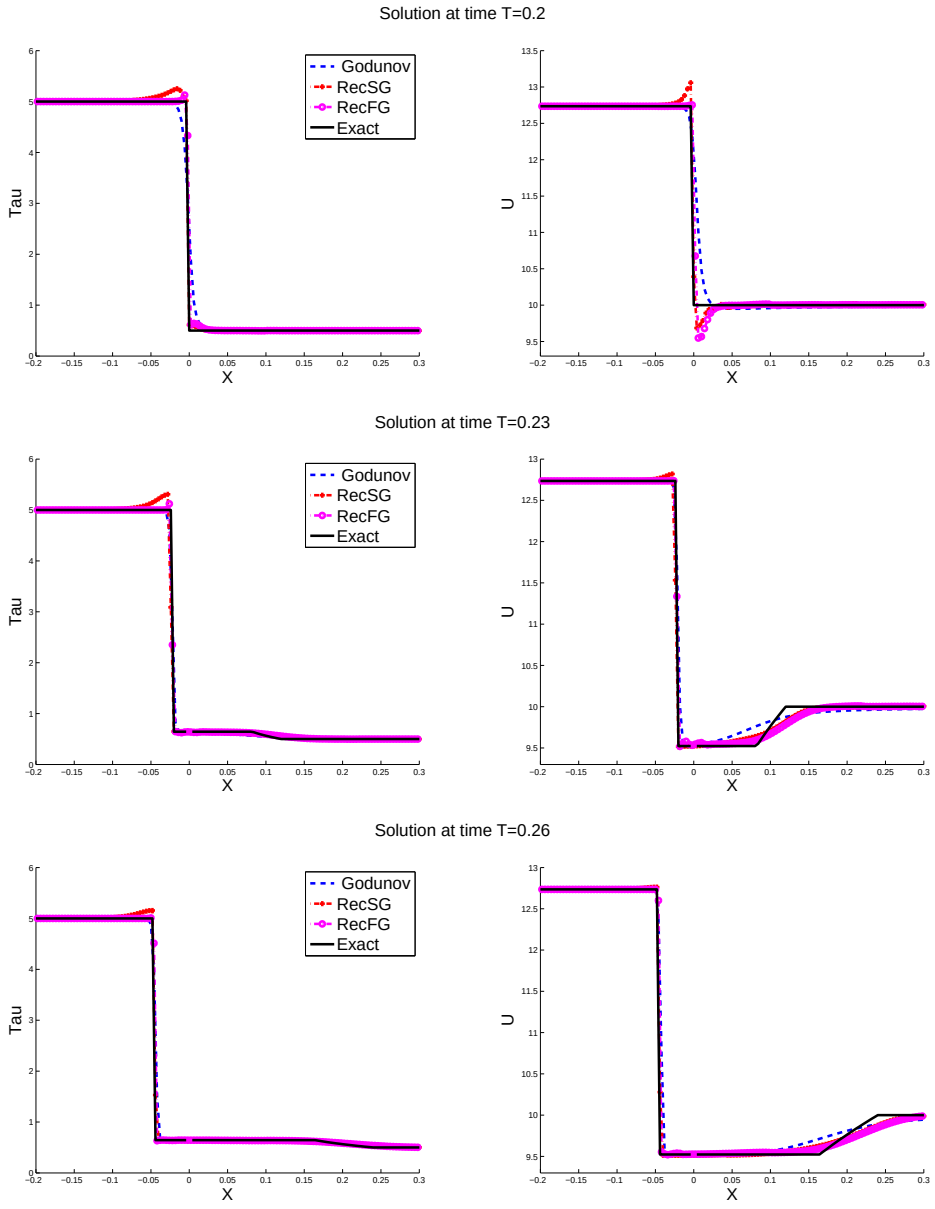

Figure 12: Solution of test 5 with, from top to bottom, $t = 0.2$, $t = 0.22$ and $t = 0.26$.

test case. More precisely, we plot the evolution of the quantity

$$\int \mathcal{U}(\tau^n_{\rm rec}(x), u^n_{\rm rec}(x))dx - \int \mathcal{U}(\tau^{n-1}_{\rm rec}(x), u^{n-1}_{\rm rec}(x))dx$$
$$+ (t^n - t^{n-1})((\mathcal{W}(\tau_R, u_R) - V^{n-1}_{\rm mesh}\mathcal{U}(\tau_R, u_R)) - (\mathcal{W}(\tau_L, u_L) - V^{n-1}_{\rm mesh}\mathcal{U}(\tau_L, u_L)))$$

where

$$\tau^n_{\rm rec}(x) = \sum_j (\tau^n_{j,L}\mathbf{1}_{x<x^n_{j-1/2}+d^{n,\tau}_j} + \tau^n_{j,R}\mathbf{1}_{x\geq x^n_{j-1/2}+d^{n,\tau}_j})\mathbf{1}_{x\in[x^n_{j-1/2},x^n_{j+1/2}]}$$

and

$$u^n_{\rm rec}(x) = \sum_j (u^n_{j,L}\mathbf{1}_{x<x^n_{j-1/2}+d^{n,u}_j} + u^n_{j,R}\mathbf{1}_{x\geq x^n_{j-1/2}+d^{n,u}_j})\mathbf{1}_{x\in[x^n_{j-1/2},x^n_{j+1/2}]}$$

are the reconstructed solution at time t^n (we recall than on a fixed grid, $V^{n-1}_{\rm mesh} = 0$ for all n).

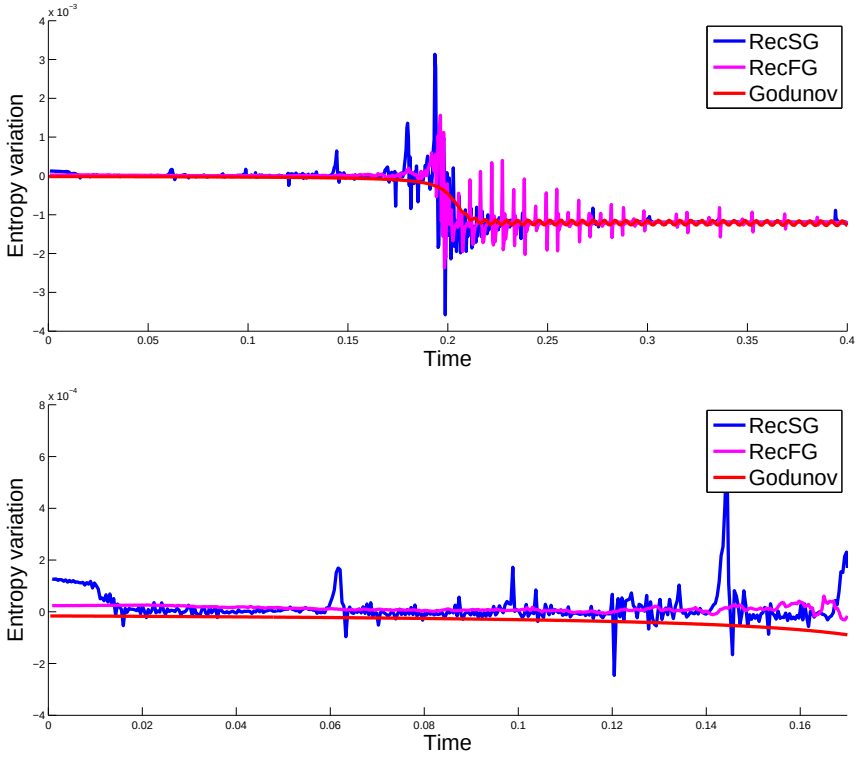

Figure 13: Evolution of the entropy through time in test 5, on the time interval $[0, 4]$ (top), and a zoom before time $T_{\rm rar}$ (bottom).

On Figure 13, we can see that this quantity oscillates around 0 and often takes positive values until the time $T_{\rm rar} = 0.2$. It indicates that the scheme is not entropy satisfying in the strict sense, but only in a "weak" sense to be defined. Indeed, the scheme seems to

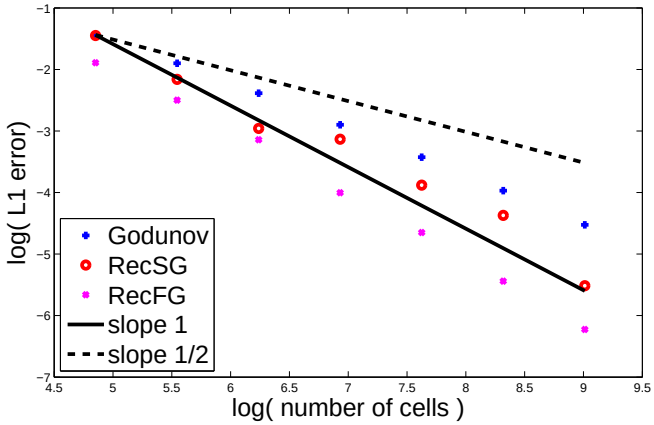

Figure 14: L^1-error at time $T_{\rm rar}$ with the Godunov-type scheme and with the discontinuous reconstruction schemes.

converge toward the correct solution for the L^1-norm. The order of convergence is plotted on Figure 14.

Note also that even though the scheme is not entropy satisfying, it contains entropy information as the underlying approximate Riemann solver of [CC14] is entropy satisfying. It is thus likely that the problem comes from the discontinuous reconstruction strategy. More precisely, we believe that some reconstructions are not entropy satisfying and should be cancelled using a stronger constraint than the ones proposed in (21)-(22) (i.e. $d_j^{n,\tau} \in [0, \Delta x]$ and $d_j^{n,u} \in [0, \Delta x]$). For example in this case, we expect the reconstructed solution $U_{\rm rec}^n = (\tau_{\rm rec}^n, u_{\rm rec}^n)$ to be monotonous for times $t < T_{\rm rar}$, but as depicted on Figure 15, this is not the case at all in the course of the first iteration ($n = 0$).

In the scalar case, entropy satisfying versions of the anti-diffusive scheme of [DL01] (which can be reinterpreted in terms of discontinuous reconstruction) have been proposed in [Bou04a], but remain to be adapted to the present setting. It is a challenging and open problem at the stage of the present work.

3 Two dimensional simulation

In two space dimensions, the p-system writes

$$\begin{cases} \partial_t \tau - \partial_x u - \partial_y v = 0, \\ \partial_t u + \partial_x p(\tau) = 0, \\ \partial_t v + \partial_y p(\tau) = 0, \\ \tau(0,x) = \tau^0(x), \ u(0,x) = u^0(x), \ v(0,x) = v^0(x). \end{cases} \tag{29}$$

The velocity of the fluid is (u, v). We use a directional splitting to approach the solution of (29). The space domain is the square $[-1, 1]^2$ with rigid walls. We take $p(\tau) = \tau^{-2}$,

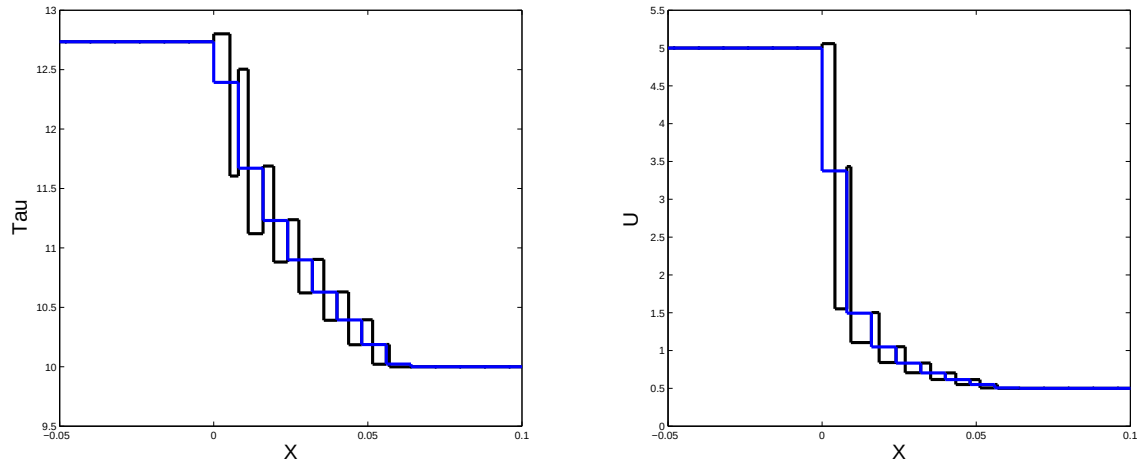

Figure 15: In black, the reconstructed solution U^0_{rec}, i.e. the solution reconstructed from the initial data before any iteration in time is done. We take $T_{\text{rar}} = 0.015$ and 500 cells. In blue, the piecewise constant function corresponding to $(U^0_j)_{j\in\ \mathbb{Z}}$

which corresponds to the pressure law for the shallow-water equation written in Lagrangian coordinates. The initial data is

$$\begin{cases} \tau^0(x,y) = \mathbf{1}_{\sqrt{x^2+y^2}\geq 0.5} + 2 * \mathbf{1}_{\sqrt{x^2+y^2}<0.5}, \\ u^0(x,y) = v^0(x,y) = 0. \end{cases}$$

We compare the solution given by the discontinuous reconstruction scheme on a fixed grid and the Godunov-type scheme at different times. The specific volume τ is represented on Figures 16, 17 and 18. In that case, it corresponds to the inverse of the height of water. The discontinuities are sharply captured with the reconstruction scheme, with much more details captured with this method.

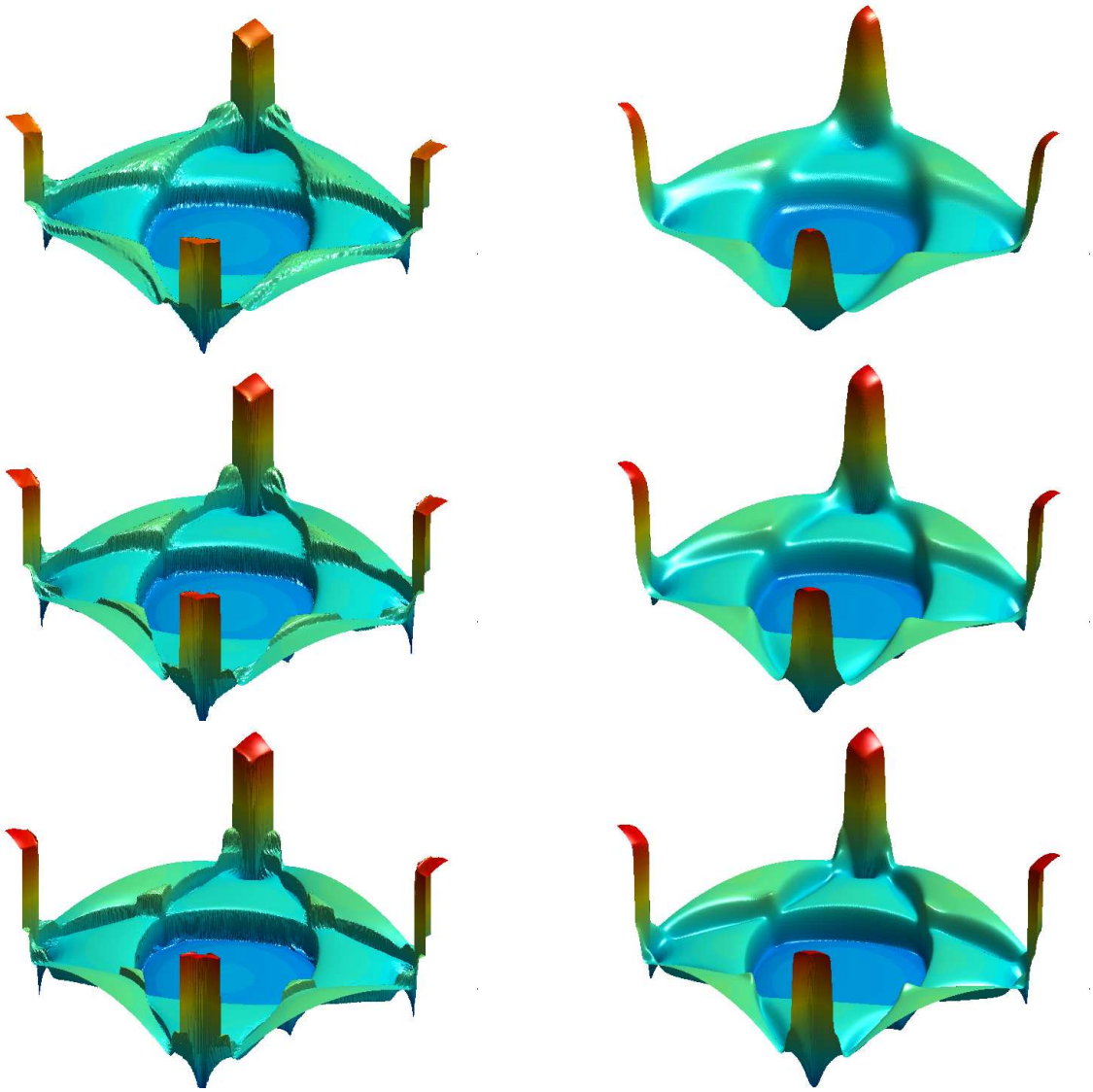

Figure 16: Comparison of τ for the discontinuous reconstruction scheme (left) and the Godunov-type scheme (right) at time $t = 3.05$ for meshes with (from top to bottom): 200×200, 400×400 and 800×800 cells

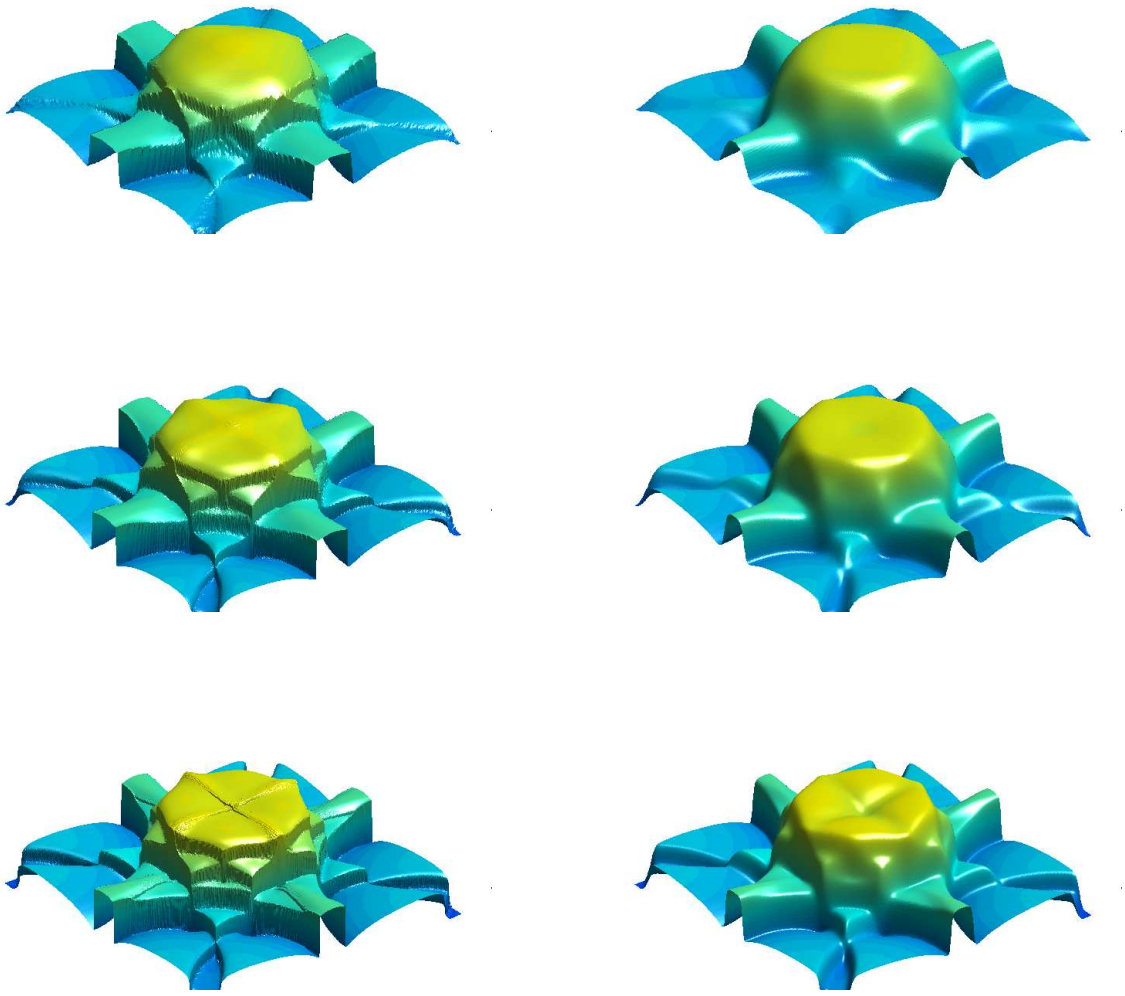

Figure 17: Comparison of τ for the discontinuous reconstruction scheme (left) and the Godunov-type scheme (right) at time $t = 3.82$ for meshes with (from top to bottom): 200×200, 400×400 and 800×800 cells.

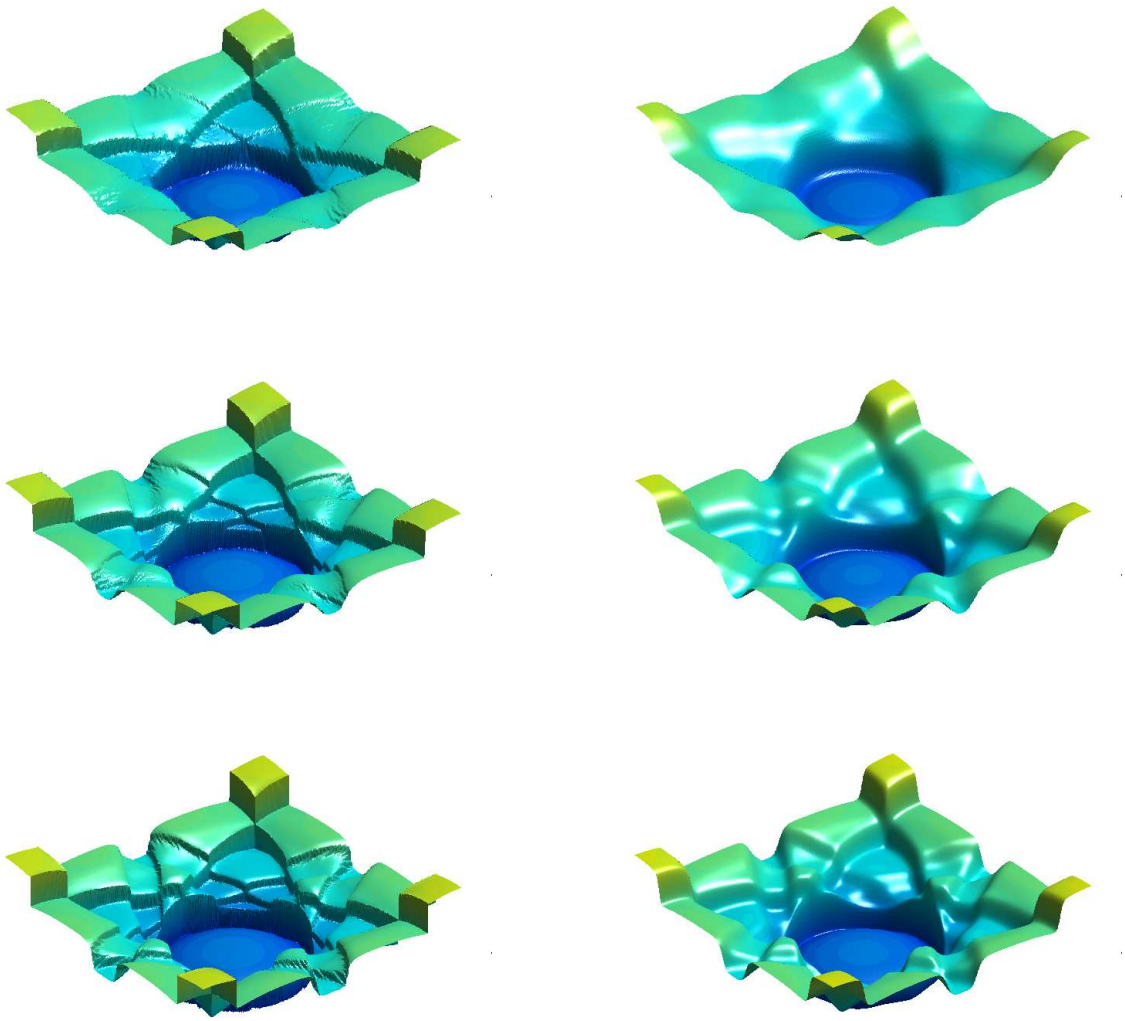

Figure 18: Comparison of τ for the discontinuous reconstruction scheme (left) and the Godunov-type scheme (right) at time $t = 4.58$ for meshes with (from top to bottom): 200×200, 400×400 and 800×800 cells.

References

[ADVLCL08] François Alouges, Florian De Vuyst, Gérard Le Coq, and Emmanuel Lorin. The reservoir technique: a way to make Godunov-type schemes zero or very low diffuse. Application to Colella-Glaz solver. *Eur. J. Mech. B Fluids*, 27(6):643–664, 2008.

[Agu14] Nina Aguillon. A reconstruction scheme for the euler equations. *Prepint, hal-00967484*, 2014.

[AR97] Mohit Arora and Philip L. Roe. On postshock oscillations due to shock capturing schemes in unsteady flows. *J. Comput. Phys.*, 130(1):25–40, 1997.

[BCLL08] Benjamin Boutin, Christophe Chalons, Frédéric Lagoutière, and Philippe G. LeFloch. Convergent and conservative schemes for nonclassical solutions based on kinetic relations. I. *Interfaces Free Bound.*, 10(3):399–421, 2008.

[BdL09] François Bouchut and Tomás Morales de Luna. Semi-discrete entropy satisfying approximate Riemann solvers. The case of the Suliciu relaxation approximation. *J. Sci. Comput.*, 41(3):483–509, 2009.

[BFBC+11] Marie Billaud Friess, Benjamin Boutin, Filipa Caetano, Gloria Faccanoni, Samuel Kokh, Frédéric Lagoutière, and Laurent Navoret. A second order antidiffusive Lagrange-remap scheme for two-component flows. In *CEMRACS'10 research achievements: numerical modeling of fusion*, volume 32 of *ESAIM Proc.*, pages 149–162. EDP Sci., Les Ulis, 2011.

[Bou04a] François Bouchut. An antidiffusive entropy scheme for monotone scalar conservation laws. *J. Sci. Comput.*, 21(1):1–30, 2004.

[Bou04b] François Bouchut. A reduced stability condition for nonlinear relaxation to conservation laws. *J. Hyperbolic Differ. Equ.*, 1(1):149–170, 2004.

[CC14] Christophe Chalons and Frederic Coquel. Modified Suliciu relaxation system and exact resolution of isolated shock waves. *Math. Models Methods Appl. Sci.*, 24(5):937–971, 2014.

[CDMG14] Christophe Chalons, Maria Laura Delle Monache, and Paola Goatin. A conservative scheme for non-classical solutions to a strongly coupled pde-ode problem a conservative scheme for non-classical solutions to a strongly coupled pde-ode problem. *Preprint*, 2014.

[CLL94] Gui Qiang Chen, C. David Levermore, and Tai-Ping Liu. Hyperbolic conservation laws with stiff relaxation terms and entropy. *Comm. Pure Appl. Math.*, 47(6):787–830, 1994.

[DL01] Bruno Després and Frédéric Lagoutière. Contact discontinuity capturing schemes for linear advection and compressible gas dynamics. *J. Sci. Comput.*, 16(4):479–524 (2002), 2001.

[God59] Sergei. K. Godunov. A difference method for numerical calculation of discontinuous solutions of the equations of hydrodynamics. *Mat. Sb. (N.S.)*, 47 (89):271–306, 1959.

[GR96] Edwige Godlewski and Pierre-Arnaud Raviart. *Numerical approximation of hyperbolic systems of conservation laws*, volume 118 of *Applied Mathematical Sciences*. Springer-Verlag, New York, 1996.

[Har89] Ami Harten. ENO schemes with subcell resolution. *J. Comput. Phys.*, 83(1):148–184, 1989.

[JX95] Shi Jin and Zhou Ping Xin. The relaxation schemes for systems of conservation laws in arbitrary space dimensions. *Comm. Pure Appl. Math.*, 48(3):235–276, 1995.

[Lag08] Frédéric Lagoutière. Stability of reconstruction schemes for scalar hyperbolic conservation laws. *Commun. Math. Sci.*, 6(1):57–70, 2008.

[LagXX] Frédéric Lagoutière. Non-dissipative entropy satisfying discontinuous reconstruction schemes for hyperbolic conservation laws. *Preprint*, XX.

[LWM08] Hongxia Li, Zhigang Wang, and De-kang Mao. Numerically neither dissipative nor compressive scheme for linear advection equation and its application to the Euler system. *J. Sci. Comput.*, 36(3):285–331, 2008.

[NT90] Haim Nessyahu and Eitan Tadmor. Nonoscillatory central differencing for hyperbolic conservation laws. *J. Comput. Phys.*, 87(2):408–463, 1990.

[Sul98] Ion Suliciu. On the thermodynamics of rate-type fluids and phase transitions. I. Rate-type fluids. *Internat. J. Engrg. Sci.*, 36(9):921–947, 1998.

[Tor09] Eleuterio F. Toro. *Riemann solvers and numerical methods for fluid dynamics*. Springer-Verlag, Berlin, third edition, 2009. A practical introduction.

[vL97] Bram van Leer. Towards the ultimate conservative difference scheme. V. A second-order sequel to Godunov's method. *J. Comput. Phys.*, 135(2):227–248, 1997.